Neurobiology of Disease

Endolysosome Localization of ERα Is Involved in the Protective Effect of 17α-Estradiol against HIV-1 gp120-Induced Neuronal Injury

Gaurav Datta,[1]* Nicole M. Miller,[1]* Wenjuan Du,[2] Jonathan D. Geiger,[1] Sulie Chang,[2] and Xuesong Chen[1]

[1]Department of Biomedical Sciences, University of North Dakota School of Medicine and Health Sciences, Grand Forks, North Dakota 58202-9037, and [2]Institute of Neuroimmune Pharmacology and Department of Biological Sciences, Seton Hall University, South Orange, New Jersey 07079

Neurotoxic HIV-1 viral proteins contribute to the development of HIV-associated neurocognitive disorder (HAND), the prevalence of which remains high (30–50%) with no effective treatment available. Estrogen is a known neuroprotective agent; however, the diverse mechanisms of estrogen action on the different types of estrogen receptors is not completely understood. In this study, we determined the extent to which and mechanisms by which 17α-estradiol (17αE2), a natural less-feminizing estrogen, offers neuroprotection against HIV-1 gp120-induced neuronal injury. Endolysosomes are important for neuronal function, and endolysosomal dysfunction contributes to HAND and other neurodegenerative disorders. In hippocampal neurons, estrogen receptor α (ERα) is localized to endolysosomes and 17αE2 acidifies endolysosomes. ERα knockdown or overexpressing an ERα mutant that is deficient in endolysosome localization prevents 17αE2-induced endolysosome acidification. Furthermore, 17αE2-induced increases in dendritic spine density depend on endolysosome localization of ERα. Pretreatment with 17αE2 protected against HIV-1 gp120-induced endolysosome deacidification and reductions in dendritic spines; such protective effects depended on endolysosome localization of ERα. In male HIV-1 transgenic rats, we show that 17αE2 treatment prevents the development of enlarged endolysosomes and reduction in dendritic spines. Our findings demonstrate a novel endolysosome-dependent pathway that governs the ERα-mediated neuroprotective actions of 17αE2, findings that might lead to the development of novel therapeutic strategies against HAND.

Key words: 17a-estradiol; dendritic spine; ERa; HIV-1 gp120; HIV-associated neurocognitive disorders; lysosome

---

Significance Statement

Extranuclear presence of membrane-bound estrogen receptors (ERs) underlie the enhancing effect of estrogen on cognition and synaptic function. The estrogen receptor subtype ERα is present on endolysosomes and plays a critical role in the enhancing effects of 17αE2 on endolysosomes and dendritic spines. These findings provide novel insight into the neuroprotective actions of estrogen. Furthermore, 17αE2 protected against HIV-1 gp120-induced endolysosome dysfunction and reductions in dendritic spines, and these protective effects of 17αE2 were mediated via endolysosome localization of ERα. Such findings provide a rationale for developing 17αE2 as a therapeutic strategy against HIV-associated neurocognitive disorders.

Introduction

Although combined antiretroviral therapy (cART) suppresses levels of HIV-1 throughout the body including in plasma and CSF, it does not eliminate the virus. The 30–50% of people living with HIV experience HIV-associated neurocognitive disorder (HAND), against which effective treatments are not available (Maschke et al., 2000; Grant et al., 2014; Sacktor et al., 2016). Synaptodendritic impairments that occurs in various brain regions including prefrontal cortex and hippocampus are the key pathologic features of HAND, and these changes correlate closely with neurocognitive impairment (Masliah et al., 1997; Everall et al., 1999; Sá et al., 2004; Ellis et al., 2007). The development of synaptodendritic impairments in HANDs in the cART era is complex and not fully understood, but may be mediated by the disruption of neuronal homeostasis because of the chronic presence of neurotoxic viral proteins, such as gp120 and Tat, along with low-grade inflammation (Gonzalez-Scarano and Martin-Garcia, 2005; Saylor et al., 2016; Raybuck et al., 2017).

Endolysosomes are especially important for neurons, because their extensive processes require constant vesicular membrane trafficking to establish and maintain axonal and somatodendritic plasma membrane domains. Being at the crossroads of transporting proteins to the dendritic spines and in the degradation of dendritic cargos, endolysosomes have been shown to be important in modulating synaptic plasticity, (Goo et al., 2017; Padamsey et al., 2017; Nikoletopoulou and Tavernarakis, 2018; Yap et al., 2018). Endolysosome dysfunction has been implicated in HAND (Gelman et al., 2005; Spector and Zhou, 2008; Zhou and Spector, 2008; Cysique et al., 2015). We and others have shown that neurotoxic HIV-1 proteins including Tat (Hui et al., 2012; Chen et al., 2013; Fields et al., 2015) and gp120 (Bae et al., 2014; Datta et al., 2019; Halcrow et al., 2021), as well as certain ART drugs (Hui et al., 2021) deacidify endolysosomes, induce the enlargement of endolysosomes, and disrupt endolysosome function. In addition, HIV-1 (Cinti et al., 2017) and other HIV-1-related factors (Moorjani et al., 1996; Campbell et al., 2015; Dagur et al., 2021; Santerre et al., 2021) also disrupt endolysosome function. Thus, endolysosome dysfunction could contribute to synaptodendritic impairments in HAND. Conversely, enhancing endolysosome function represents a promising therapeutic strategy.

Estrogen exerts an enhancing effect on cognition and synaptic function (Hojo et al., 2008; Srivastava et al., 2011; Lai et al., 2017). The extranuclear presence of membrane-bound estrogen receptors (ERs) in neurons have been implicated in estrogen's neuroprotective effects (Milner et al., 2001, 2005). These membrane-bound receptors exhibit distinct subcellular distribution patterns: ERα proteins are mainly expressed on endolysosomes (Milner et al., 2001; Sampayo et al., 2018), ERβ proteins are mainly mitochondrial (Yang et al., 2004; Milner et al., 2005; Liao et al., 2015), and G-protein coupled ER1 (GPER) proteins are mainly on endoplasmic reticulum (Revankar et al., 2005). Endolysosome localization of ERα has been implicated in its degradation (Sampayo et al., 2018). However, ERα is not a transmembrane protein, and, as a cytosolic protein, ERα can attach to the membrane via palmitoylation (Schlegel et al., 1999; Adlanmerini et al., 2014; Pedram et al., 2014). Thus, endolysosome-localized ERα most likely resides on endolysosome membranes that face cytosol rather than lumen, and membrane-permeable estrogen likely activates these receptors and initiates endolysosome-dependent actions.

In the present study, we determined the extent to which 17α-estradiol (17αE2) affects endolysosome function and dendritic spines via endolysosome-localized ERα. We demonstrated that endolysosome localization of ERα is responsible not only for 17αE2-induced endolysosome acidification and increases in dendritic spines, but also is responsible for the protective effect of 17αE2 against HIV-1 gp120-induced endolysosome dysfunction and reduction in dendritic spines.

Materials and Methods

Animals. Fisher 344 and HIV-transgenic (Tg) rats were purchased from Harlan Laboratories. They were housed with three animals per ventilated plastic cage (Animal Care Systems) and maintained in a temperature- and humidity-controlled environment. They were kept on a 12 h light/dark cycle and fed a standard rodent diet. The experimental protocol was approved by the Institutional Animal Care and Use Committee (IACUC) at Seton Hall University (South Orange, NJ). Male HIV-1 Tg rats and age-matched male F344 rats were used to determine the effect of 17αE2 on dendritic branching and spines. Male rats were chosen to minimize the effects of endogenous estradiol. Older rats were

chosen in part because endogenous estradiol levels decline as animal ages (Russell et al., 2019). Twelve-month-old male HIV-1 Tg and F344 control rats were randomly assigned into the following four groups (each group contains five animals): F344 control, F344 treated with 17αE2, HIV-1 Tg, and HIV-1 Tg treated with 17αE2. Twelve-month-old HIV-1 Tg rats were used because successful viral suppression of cART has dramatically increased the life span of people living with HIV-1 (May et al., 2014), and half of people living with HIV-1 were ≥50 years of age in the United States, because people ≥50 years of age comprise the fastest-growing age group in the HIV-positive population (Hall et al., 2008) and because advanced age increases the risk for neurocognitive impairment (Bhaskaran et al., 2008; Alford and Vera, 2018). Animals were trained to eat pure chocolate-flavored hazelnut cream with sesame oil for 5 d before daily administration with and without 17αE2 (30 μg of 17αE2/5 μl sesame oil/1 g of Nutella cream/d). This dosage of 17αE2 was based on findings that a similar dose of 17αE2 has been shown to increase life span in mice (Harrison et al., 2014, 2021; Strong et al., 2016; Garratt et al., 2017). This dosage of 17αE2 used in HIV-1 Tg rats was also adjusted based on the differences in weight and BMI between mice and rats (Reagan-Shaw et al., 2008; Massud et al., 2015). The feeding duration was continued for a total of 21 d, and on day 22 rats were perfused with 4% paraformaldehyde (PFA) and the brains were collected for Golgi–Cox staining and immunohistochemistry.

Cell cultures. The mouse embryonic hippocampal E-18 cell line CLU199 (Cellutions Biosystems) was grown and maintained in 1× DMEM with 10% fetal bovine serum, 25 mM glucose, and 1% penicillin/streptomycin, at 37°C with 5% CO_2 following manufacturer instructions. For all experiments in this study, only cells from passages 3–7 were used. Primary mouse embryonic hippocampal neurons (E18) were obtained from E18 mouse cortex (C57EHP, BrainBits) following standard primary neuron culture protocols and manufacturer instructions. Briefly, the tissue was digested with papain for 10 min and plated at 100,000 cells/well on either 12 mm poly-D-lysine coverslips (GG-12-PDL, Neuvitro Corporation) in 24-well plates or on 35 mm poly-D-lysine-coated glass bottom dishes (P35GC-0–10-C, MatTek Life Sciences). NbActiv media (BrainBits) were used for both plating and maintenance, and neuronal cultures were incubated at 37°C with 5% CO_2 with half the media exchanged every 3–4 d.

Live imaging of dendritic spines. Mouse primary hippocampal neurons [day *in vitro* (DIV) 12–14] were transduced with GFP (BacMam GFP; catalog #B10383, Thermo Fisher Scientific) for 48 h following manufacturer recommendations. Before imaging, neurons were transferred to warm (37°C) Hibernate E. Low Fluorescence (HELF) medium (Brainbits) on a confocal microscope (catalog #LSM800, Zeiss) for imaging. Once a field under a 63× objective was chosen for imaging, monomeric recombinant HIV-1 IIIB gp120 protein (ImmunoDx), heat-inactivated HIV-1 gp120 (95°C for 1 h), and 17αE2 (Tocris Bioscience) were added according to experiment design, and neurons were imaged continuously (1 min intervals) for 10 min with z-stack intervals of 0.5 μm. The dendritic spines at 0 min ($t – 0$) and 10 min ($t – 10$) were reconstructed with Imaris 9.5 using the filaments module and plotted as a percentage of spines lost/gained. A total of 7–10 neurons comprising >5000 spines were imaged per treatment, and experiments were repeated independently three times with different cultures. The criteria for spine classification were the same as in earlier published studies (Christensen et al., 2011).

Immunostaining. Neurons (DIV 14–17) were treated, briefly rinsed in PBS, and fixed with 4% PFA in 4% sucrose for 20 min at room temperature (RT) and then washed in PBS three times. Neurons were permeabilized with 0.1% Triton X-100 for 10 min, incubated in blocking buffer [3% BSA (Sigma-Aldrich) with 1% goat or donkey serum (Thermo Fisher Scientific) in PBS] for 1 h, then incubated with primary antibodies at 4°C overnight. After one wash with PBST (PBS, Tween20–0.1%) and two PBS washes, secondary antibodies were added for 1 h at 4°C. Cells were then washed and mounted on microscope slides (Thermo Fisher Scientific) with ProLong Gold Antifade (catalog #P36930, Thermo Fisher Scientific). The following primary antibodies were used in immunofluorescence staining: ERα (1:50; catalog #sc-8002,

Santa Cruz Biotechnology); LAMP1 (D2D11; 1:500; catalog #9091S, Cell Signaling Technology); Rab7 (1:500; catalog #ab137029, Abcam); PSD-95 (1:500; catalog #ab13552, Abcam); and MAP2 (1:500; catalog #ab32454, Abcam). Alexa Fluor 594 goat anti-rabbit, Alexa Fluor 488 goat anti-rabbit, Alexa Fluor 594 goat anti-mouse, and Alexa Fluor 488 goat anti-mouse secondary antibodies were from Thermo Fisher Scientific. All secondary antibodies were used at a 1:500 dilution. Controls for immunostaining specificity included staining cells with primary antibodies without fluorescence-conjugated secondary antibodies (background controls), and staining cells with only secondary antibodies; these controls helped eliminate autofluorescence in each channel and bleed-through (crossover) between channels.

Endolysosomal pH measurement. Total endolysosomal pH measurement was performed in CLU199 cells using a combination of dextran labeling, as done previously (Nash et al., 2019). Briefly, CLU199 cells were plated on 35 mm glass bottom poly-D-lysine dishes, and after 24 h loaded with 10 μg/ml each of pH-sensitive pHrodo Green Dextran (catalog #P35368, Thermo Fisher Scientific) and pH-insensitive dextran, Texas Red (D1863, Thermo Fisher Scientific) for another 24 h. The following morning, dextran containing medium was washed off twice with PBS, and cells were transferred to Hibernate E. Low Fluorescence (HELF) medium (Brainbits) at 37°C for imaging. HIV-1 gp120, heat-inactivated gp120, or 17αE2 was added at the mentioned concentrations and fluorescence emission at 533 and 615 nm measured for Green and Texas Red dextran, respectively. The ratio of 615:533 was converted to pH using an intracellular pH calibration kit (catalog #P35379, Thermo Fisher Scientific) with the addition of 10 μM nigericin and 20 μM monensin in HELF medium adjusted to different pH values with HCl or NaOH. For specific measurement of Rab7 vesicle pH, CLU199 cells were loaded with the combination of pH-sensitive and pH-insensitive dextran, as described above, for 6 h, following which the cells were washed and placed in fresh growth media for 2 h before being transferred to HELF medium for imaging. This dextran loading method was optimized as per earlier experiments to maximize the loading of dextran into Rab7 vesicles. For all pH imaging and measurements, a total of five fields under 40× magnification on a confocal microscope (catalog #LSM800, Zeiss) comprising at least 5–10 cells/field were imaged, and three independent experiments were conducted.

Immunohistochemistry. Perfusion-fixed (4% PFA) rat brains were removed, postfixed overnight at 4°C, cryoprotected with 30% sucrose, and cut on a cryostat (catalog #CM1520, Leica) into 10 μm sagittal sections. The slides were then stored in −80°C freezer until further use. Before staining, the slides were thawed overnight at 4°C, washed in PBS, and blocked for 1 h in blocking solution (3% BSA, 1% normal goat serum, and 0.05 Triton X-100). Primary antibodies were then added and kept overnight at 4°C. The following primary antibodies were used: MAP2 (1:100; catalog #92434, Abcam); LAMP1 (1:100; catalog #24170, Abcam); Rab7 (1:100; catalog #ab126712, Abcam); and ERα (1:50; catalog #sc-8002, Santa Cruz Biotechnology). The following day, primary antibodies were washed out with two PBS-T washes (Tween0.01%) and two PBS washes, each for 5 min. Secondary antibodies (Alexa Fluor 488 and Alexa Fluor 594) were then added for 1 h at 4°C, following which slides were washed, and coverslips were mounted with Vectashield Antifade Mounting Medium with DAPI (catalog #H-1200, Vector Laboratories). The 0.5-μm-interval z-stack images were acquired on a confocal microscope (catalog #LSM800, Zeiss) using the ZEN acquisition software, and images were analyzed to calculate colocalization and lysosome volume in Imaris 9.6 (Bitplane). Lysosome volume was calculated by recreating the LAMP1 staining as spots using the spot module in Imaris 9.6. Colocalization of ERα with Rab7 and LAMP1 was calculated using the colocalization module after adjusting the threshold in Imaris 9.6.

Golgi–Cox staining. The Golgi–Cox method used was adapted from studies by Risher et al. (2014), Du (2019), and Zhong et al. (2019) with slight modifications. The Golgi–Cox method was chosen for labeling dendritic spines because it is much simpler compared with the DiOlistic method, which requires specialized equipment (McLaurin et al., 2018). The brain was cut into two hemispheres and placed in Golgi–Cox solution for 24 h at RT in dark for impregnation. After 24 h, the brains were

moved to fresh Golgi–Cox stain for another 10 d at RT followed by transfer to a tissue protectant solution for 24 h at 4°C, and then to fresh tissue protectant solution at 4°C in the dark for another 7 d. The brains were then transferred to molds, sectioned into 100 μm sections using a vibratome (Leica), and mounted onto gelatin-coated microscopic slides. For staining, the slides were washed twice with distilled water (DW) and incubated in 20% ammonia solution for 10 min in the dark with gentle shaking, followed by two DW washes of 5 min each. The sections were then rinsed in 1% sodium thiosulfate solution with gentle shaking for 10 min and followed by two DW washes of 5 min each. Slides were finally dehydrated by sequential passage through ethanol (50%, 75%, 90%, and 100% twice), cleared in xylene (twice, 5 min each), and mounted with Permount mounting medium (catalog #SP15-100, Thermo Fisher Scientific). Bright-field images under 100×, 63×, and 5× objectives with 0.1 μm z-stacks were acquired using an upright microscope (catalog #BX-63, Olympus), and images were analyzed with Neurolucida 360 software (MBF Bioscience). In Neurolucida 360, only complete neurons with soma and dendrites visible were imaged wherein soma were manually added, dendrites were detected with user-guided tracing mode, and spines were automatically detected with manual adjustments for each dendrite. Spine classification parameters were adjusted to be the same as used for primary cultured neurons in Imaris. The neuron tracing data were saved, transferred to Neurolucida Explorer for analysis, and exported to Excel.

Cathepsin D staining. Active levels of cathepsin D (CatD) in both CLU199 cells and primary neurons were measured using BODIPY-FL Pepstatin A (catalog #P12271, Thermo Fisher Scientific), which is based on the binding of pepstatin A to cathepsin D. LysoTracker Red DND-99 (10 nM) was added along with BODIPY-FL Pepstatin A (1 μM for 30 min in growth media) at 37°C and followed by two PBS washes, and were shifted to HELF media for immediate imaging. A total of 25–30 cells were imaged using a confocal microscope (model LSM 800, Zeiss) per treatment group using 0.5 μm z-stack intervals, and experiments were repeated three times independently. Total endolysosomes using LysoTracker Red and cathepsin D-positive endolysosomes using BODIPY-FL Pepstatin A were reconstructed as spots in Imaris 9.6 (Bitplane), and object-based colocalization was conducted using a distance of 0.2 μm.

Plasmid transfections, transductions, and siRNA knockdown. The plasmids ERα-GFP (MG227304), ERα C451A-GFP, ERα-HA, and ERα C451A-HA were all obtained from Origene Technologies along with custom modifications. The plasmids were cloned into pCMV6-AC-GFP, pCMV6-AC-RFP, or pCMV6-AC-3HA vectors for GFP, RFP, and HA tag additions, respectively. For transient plasmid transfections, CLU199 cells were split onto 35 mm poly-D-lysine-coated glass bottom dishes or 12 mm poly-D-lysine coverslips, and on reaching 50% confluency were transfected with 2 μg of plasmid DNA and Lipofectamine 2000 transfection Reagent (catalog #11668019, Thermo Fisher Scientific) in Opti-MEM Reduced Serum media (catalog #31985062, Thermo Fisher Scientific) for 48–72 h following which they were assayed and imaged. Primary mouse hippocampal neurons were transiently transfected with 1 μg of plasmid DNA and Lipofectamine 2000 on DIV 5–7 for 48 h before imaging on DIV 7–9. For primary neurons, the media were changed 4 h after transfection with preconditioned media.

On-Target plus mouse Esr1 (Entrez Gene ID, 13982) siRNA-SMART pool to knock down (KD) ERα was obtained from Dharmacon with the following target sequences: CCUACUACCUGGAGAACGA, GAAAGGCGGCAUACGGAAA, GUCCAGCAGUAACGAGAAA, and GGGCUAAAUCUUGGUAACA. For siRNA transfections, siRNA was dissolved in Accell1 transfection medium (catalog #B-005000, Dharmacon) and DharmaFECT 1 (catalog #T-2001–02, Dharmacon) was used as transfection reagent for both CLU199 cells and primary neurons (DIV 7–9). The final siRNA concentration was 50 nM for both CLU199 cells and primary neurons.

Nuclear activation of ER. Nuclear activation of ER was performed by the TransAM ER assay (Active Motif) following manufacturer instructions with minor modifications. Briefly, 3–5 million confluent CLU199 cells were treated for 30 min, washed twice with ice-cold PBS, resuspended in 1 ml of HB buffer, and incubated for 20 min. A 0.5% solution

of NP-40 (Sigma-Aldrich) was added to the buffer, and the cells were vortexed at high speed for 15 s and then centrifuged at 3000 rpm for 10 min to separate the cytoplasmic (supernatant) and nuclear (pellet) fractions. The pellet was dissolved in 50 µl of lysis buffer and kept on an incubator for 30 min at 4°C, following which it was centrifuged at 14,000 rpm for 15 min to get the nuclear extract. Protein estimation was conducted using Precision Red Advanced Protein Assay (catalog #ADV02, Cytoskeleton). The TransAM-ER ELISA using this nuclear extract was conducted without any modifications. The absorbance was measured at 450 nm in a Spectra Max Plate Reader (Molecular Devices).

Immunoblotting. CLU199 cells or primary mouse hippocampal neurons were plated on poly-D-lysine-coated six-well plates at 1×10^6 or 0.5×10^6 cells/well, respectively, for each sample. Cells were treated, harvested, and lysed in $1\times$ RIPA lysis buffer (Thermo Fisher Scientific) plus 10 mM NaF, 1 mM Na_3VO_4, and Protease Inhibitor Cocktail (Thermo Fisher Scientific). After centrifugation ($13,000 \times g$ for 10 min at 4°C), supernatants were collected, and protein concentrations were determined with a DC (detergent compatible) protein assay (BIO-RAD). Proteins (20 µg) were separated by SDS-PAGE (4–20% gel) and transferred to polyvinylidene difluoride membranes (Millipore). The membranes were incubated overnight at 4°C with appropriate primary and secondary antibodies in LI-COR blocking solution (TBS) with two TBS-Tween and TBS washes (5 min each) after every step. The blots were developed with enhanced chemiluminescence, and bands were visualized and analyzed by LI-COR Odyssey Fc Imaging System.

Experimental design and statistical analysis. All data values are shown as the mean ± SEM. The details of the *n* for each experiment is specified in the respective figure legend. All data were statistically analyzed and prepared in GraphPad Prism 9.0 software (GraphPad Software). Statistical significance between groups was determined by Student's *t* test (two-tailed), one-way ANOVA with Tukey's *post hoc* tests, or two-way ANOVA with Tukey's *post hoc* tests. Statistical significance was set at $p = 0.05$. Interaction values of each ANOVA, including *F* (DFn, DFd) and *p* values for each figure are shown in Table 1.

Results

17αe2 protects against dendritic spine impairment in HIV-1 transgenic rats

It is known that HIV-1-associated cognitive impairments show sex-specific progression (Sundermann et al., 2018; Rubin et al., 2019). Since hippocampal memory is associated with estrogen levels, the sharp increase in neurocognitive impairments in HIV-positive postmenopausal women could probably be explained by the declining neuroprotection offered by estrogen (Maki et al., 2021). Experimental studies have shown that estrogen is protective against HIV-1 infection (Wilson et al., 2006; Heron et al., 2009; Szotek et al., 2013), HIV-1 protein-induced (gp120 and Tat) neuronal cell death (Bruce-Keller et al., 2001; Corasaniti et al., 2005; Zemlyak et al., 2005; Bertrand et al., 2014), and HIV-1 associated neuropathology (Howells et al., 2019). However, most of these studies have focused on 17βE2, the therapeutic use of which is limited by its association with increased risk of breast cancer (D'Alonzo et al., 2019), thromboembolism (Cushman et al., 2018), coronary heart disease, and stroke (Bassuk and Manson, 2016).

Furthermore, the feminizing effect of 17βE2 limits its possible use in the larger general population (Moos et al., 2009; Stout et al., 2017). Thus, the present study focuses on 17αE2, the naturally occurring isomer of 17βE2. Compared with 17βE2, 17αE2 has fewer feminizing effects (Stout et al., 2017) and has been shown to be the predominant form of estrogen in brain (Toran-Allerand et al., 2005; Ikeda et al., 2015; Prokai-Tatrai and Prokai, 2019), with its brain levels unaffected by gonadectomy (Toran-Allerand et al., 2005). Here, we determined the effect of 17αE2 on dendritic spines in HIV-1 Tg rats.

Table 1. Summary of statistical analysis

Figure	Test used	Sample size	Degrees of freedom, *p* value, *t* value
1B	Two-way ANOVA	55–70/5	$F_{(1,246)} = 49.22$, $p < 0.0001$
1C	Two-way ANOVA	55–70/5	$F_{(1,246)} = 195.6$, $p < 0.0001$
1D	Two-way ANOVA	55–70/5	$F_{(1,246)} = 44.58$, $p < 0.0001$
1E	Two-way ANOVA	55–70/5	$F_{(1,246)} = 500.6$, $p < 0.0001$
2B	One-way ANOVA	3/3	$F_{(3,8)} = 10.03$, $p = 0.0044$
	One-way ANOVA	3/3	$F_{(3,8)} = 19.84$, $p = 0.0005$
2D	Two-way ANOVA	200/3	$F_{(1,764)} = 11.70$, $p = 0.0007$
	Two-way ANOVA	200/3	$F_{(1,764)} = 54.61$, $p < 0.0001$
	Two-way ANOVA	200/3	$F_{(1,764)} = 63.75$, $p < 0.0001$
	Two-way ANOVA	200/3	$F_{(1,764)} = 15.28$, $p = 0.0001$
2E	Two-way ANOVA	5/5	$F_{(1,16)} = 1.910$, $p = 0.1866$
	Two-way ANOVA	5/5	$F_{(1,16)} = 0.5001$, $p = 0.4896$
	Two-way ANOVA	5/5	$F_{(1,16)} = 5.224$, $p = 0.0363$
	Two-way ANOVA	5/5	$F_{(1,16)} = 2.173$, $p = 0.1599$
2G	One-way ANOVA	2/2	$F_{(2,3)} = 5.322$, $p = 0.1031$
3A	Two-way ANOVA	3/3	$F_{(1,8)} = 0.6959$, $p = 0.4284$
3B	Two-way ANOVA	5/5	$F_{(1,16)} = 0.01770$, $p = 0.8958$
3C	Two-way ANOVA	5/5	$F_{(1,16)} = 12.50$, $p = 0.0028$
4A	*t* test	3/3	$t = 27.39$, df = 8, $p < 0.0001$
4C	*t* test	3/3	$t = 4.2$, df = 7.812, $p = 0.0032$
5A	*t* test	3/3	$t = 9.115$, df = 1.748, $p = 0.0178$
5B	Two-way ANOVA	3/3	$F_{(1,8)} = 20.26$, $p = 0.0020$
	t test	3/3	$t = 8.916$, df = 2, $p = 0.0138$
5C	Two-way ANOVA	3/3	$F_{(1,8)} = 59.82$, $p < 0.0001$
	t test	3/3	$t = 8.412$, df = 2, $p = 0.0123$
5E	Two-way ANOVA	7/3	$F_{(1,20)} = 8.998$, $p = 0.0071$
	t test	3	$t = 48.36$, df = 2
6B	*t* test	4/4	$t = 4.753$, df = 6
6C	Two-way ANOVA	5/5	$F_{(1,16)} = 4.110$, $p = 0.0596$
	t test	5/5	$t = 4.006$, df = 4, $p = 0.0293$
6D	Two-way ANOVA	4/4	$F_{(1,12)} = 85.28$, $p < 0.0001$
	t test	4/4	$t = 9.392$, df = 3, $p = 0.0026$
6E	Two-way ANOVA	4/4	$F_{(1,12)} = 68.52$, $p < 0.0001$
	t test	4/4	$t = 11.89$, df = 3, $p = 0.0013$
7B	Two-way ANOVA	3/3	$F_{(1,8)} = 39.50$, $p = 0.0002$
	t test	3/3	$t = 4.663$, df = 2, $p = 0.0169$
8A	Two-way ANOVA	3/3	$F_{(1,8)} = 39.50$, $p = 0.0002$
	t test	3/3	$t = 4.663$, df = 2, $p = 0.0430$
8B	Two-way ANOVA	3/3	$F_{(1,8)} = 14.39$, $p = 0.0053$
	t test	3/3	$t = 6.624$, df = 2, $p = 0.0132$

This table summarizes methods of statistical analysis, degree of freedom, and significance for each figure. Tukey's multiple-comparisons test was performed *post hoc* for all ANOVAs, and two-tailed analyses were used for all Student's *t* tests.

The noninfectious HIV-1 Tg rats, which contain a gap-pol deleted provirus (Reid et al., 2001), are being increasingly used for in HAND research, because HIV-1 Tg rats mimic HAND in humans with cART. HIV-1 Tg rats express seven of the nine HIV-1 proteins (with gag-pol deleted) including gp120, Tat, and nef. Similar to those HIV-1-infected individuals receiving suppressive cART treatment (Santosuosso et al., 2009; Johnson et al., 2013; Olivetta et al., 2016; Henderson et al., 2019), low levels of these viral proteins are expressed in the brains of HIV-1 Tg rats (Reid et al., 2016). Similar to those observed in patients with HAND, HIV-1 Tg rats exhibits inflammatory and neuropathological features. HIV-1 Tg rats have been shown to exhibit HAND-like gene expression profiles, synaptodendritic damage in various brain regions (hippocampus, striatum, and prefrontal cortex), as well as behavioral deficits (Reid et al., 2001, 2016; Festa et al., 2015; McLaurin et al., 2018). Furthermore, the non-infectious HIV-1 Tg model recapitulates other important features of cART-treated HIV patients, such as immune dysregulation and controlled viral replication (Peng et al., 2010).
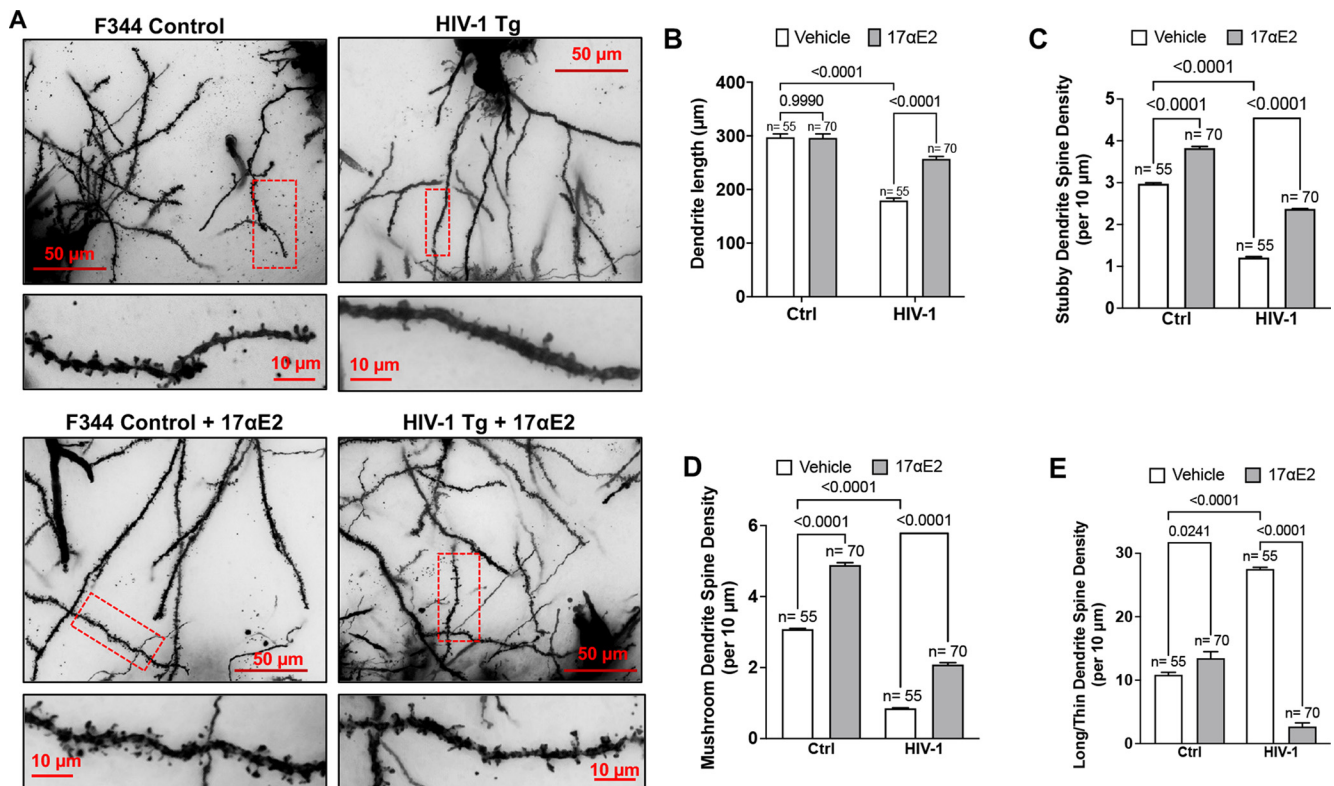
Figure 1. 17αE2 treatment protects against dendritic damage in HIV-1 transgenic rats. ***A***, Golgi–Cox staining of dendritic arborization and dendritic spine density in hippocampi of male HIV-1 Tg rats compared with F344 control (Ctrl) rats. Dendritic shafts within red boxes are enlarged in the bottom panel showing the distribution and type of spines. ***B–E***, Quantification of dendritic length (***B***), density of stubby dendritic spines (***C***), density of mushroom dendritic spines (***D***), and density of long/thin dendritic spines (***E***). *N* shows the number of neurons analyzed from at least 30 images from different hippocampus regions from five animals in each group.

Using Golgi–Cox staining in HIV-1 Tg and F344 Control rats, fed with or without 17αE2, we characterized the dendritic spine subtypes using the 3D reconstruction software Neurolucida 360 and classified them according to established protocols (Ruszczycki et al., 2012), as shown in Figure 1*A*. The hippocampal neurons of HIV-1 Tg rats exhibited decreased dendrite length (Fig. 1*B*) and altered dendritic spine density (Fig. 1*C–E*) with decreased density of stubby and mushroom spines but increased long/thin spines, which are results that are consistent with other findings that HIV-1 Tg rats exhibit the more immature subtypes of dendritic spines (McLaurin et al., 2018). 17αE2 also showed a positive spinogenesis effect in increasing the density of both stubby and mushroom spines, in agreement with earlier studies (Fig. 1*C–E*; Sengupta et al., 2019). In the HIV-1 Tg rats, 17αE2 not only attenuated decreases in dendritic length (Fig. 1*B*), but also compensated for the density of stubby, mushroom, and long/thin spines (Fig. 1*C–E*). These results confirmed the positive spinogenesis role of 17αE2.

17αe2 protects against HIV-1 gp120-induced impairment in dendritic spines
HIV-1 Tg rats mimic HAND in humans with cART, and neurologic complications in HIV-1 Tg rats have been attributed to the chronic presence of low levels of neurotoxic HIV-1 viral proteins including Tat and gp120, both of which exerts robust neurotoxic effects. Here, we chose gp120, which is well known to induce synaptodendritic impairments (Festa et al., 2015; Speidell et al., 2019), to determine the neuroprotective effects of 17αE2. HIV-1 gp120, an envelope protein that can be shed from infected cells

(Schneider et al., 1986; Moore et al., 1990), and it can be detected in body fluids (Oh et al., 1992; Klasse and Moore, 2004; Santosuosso et al., 2009) and brain (Keys et al., 1993; Trujillo et al., 1996; Nath et al., 2000). On HIV-1 virion membrane, gp120 and gp41 interact to form a trimer of gp120/gp41 heterodimer (Pancera et al., 2010). However, when shed from infected cells, gp120 exists as a soluble monomer (Moore et al., 1990; Kovacs et al., 2012). Thus, monomeric recombinant gp120 was used in our study. Here, we determined the direct effect of gp120 on dendritic morphology in mouse primary hippocampal neuronal cultures. Consistent with other findings (Festa et al., 2015; Speidell et al., 2019), gp120 treatment for 48 h decreased dendritic length and reduced dendritic spine density in a concentration-dependent effect (Fig. 2*A,B*). Based on this study, a gp120 concentration of 0.5 nM was used in all additional experiments.

Using this gp120-induced dendritic impairment model, we determined that the neuroprotective actions of 17αE2 in mouse primary hippocampal neurons (DIV 12–14) transduced with cytosolic GFP. Findings from our preliminary concentration-dependent studies as well as published reports (Mukai et al., 2007; Hasegawa et al., 2015) indicate that 17αE2 at a concentration of 10 nM exhibits a robust neuroprotective effect. Thus, neurons pretreated with 17αE2 at 10 nM for 10 min were monitored for dynamic spine changes by time-lapse imaging in the presence of gp120 (0.5 nM) treatment for 10 min. The same dendritic spines were imaged at 0 and 10 min of gp120 treatment, and the dendritic spine turnover was analyzed (Fig. 2*C*). Dendritic spine turnover was calculated as net gain/loss in different types of spines over the 10 min treatment window and shown as percentage.
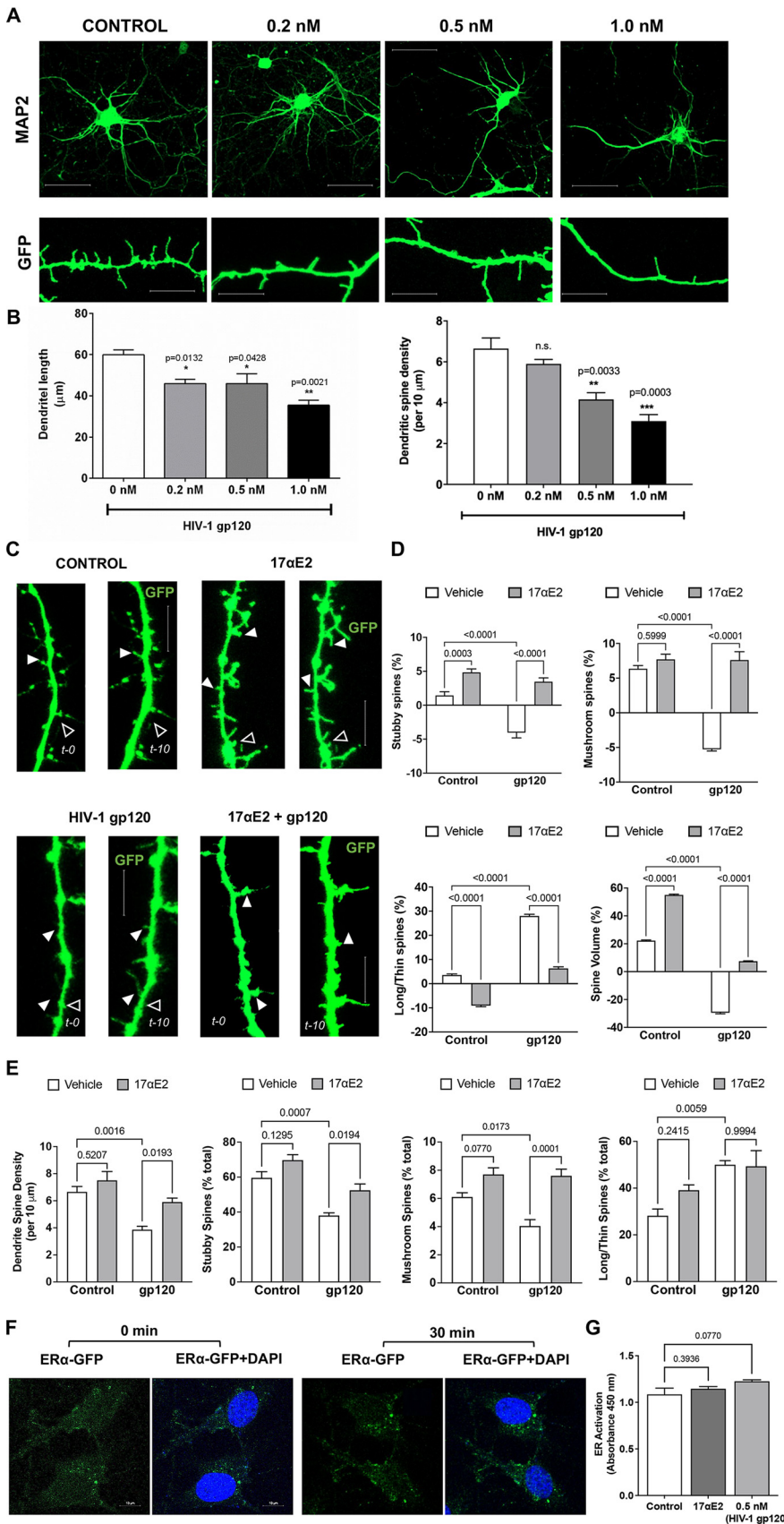
Figure 2. 17αE2 protects against HIV-1 gp120-induced dendritic damage. *A*, *B*, MAP2 staining (top; scale bar, 20 μm) and GFP expression (bottom; scale bar, 10 μm) in primary hippocampal neurons (DIV 15) after treatment with HIV-1 gp120 (0.2–1 nM for 48 h). HIV-1 gp120, in a concentration-dependent manner, decreased dendritic length and dendritic spine density. *C*, *D*, Time-lapse confocal images show the rapid changes in spine structure of the same dendrite at 0 and 10 min

As shown in Figure 2D, a reduction in stubby and mushroom spine density opposed to increased density of long/thin spines was observed with gp120, and these effects were blocked by 17αE2 pretreatment. Treatment with gp120 also resulted in a significant decrease in dendritic spine volume, which was blocked by 17αE2 pretreatment (Fig. 2D). 17αE2 treatment alone significantly promoted the formation of both stubby and mushroom spines and increased dendritic spine volume (Fig. 2D). In parallel, we determined the protective effects of 17αE2 pretreatment for 10 min against dendritic impairment induced by HIV-1 gp120 treatment (0.5 nM) for 30 min (Fig. 2E). The same trend of reduced stubby and mushroom spine density with increased long/thin spines as in our 10 min treatment was observed. These results show that 17αE2 is able to rapidly modulate dendritic spine plasticity of primary hippocampal neurons and block HIV-1 gp120-induced dendritic impairment.

Two different mechanisms of estradiol action on neurons have been demonstrated: the classical genomic or transcriptional pathway (which takes hours to days) and the rapid membrane-associated action (takes minutes to hours). Both of these pathways promote spine growth and synapse formation in brain regions including the hippocampus and the cortex (Li et al., 2004; Mendez et al., 2011; Hasegawa et al., 2015). Using a TransAM ER ELISA, we demonstrated that neither 17αE2 (10 nM) nor HIV-1 gp120 (0.5 nM) treatment for 30 min resulted in nuclear ER activation (Fig. 2F,G). These findings suggest that the short-term effect of 17αE2 on modulation of dendritic spine plasticity and the protective effects against gp120-

←

following HIV-1 gp120 treatment (0.5 nM) in the absence and presence of 17αE2 (10 nM, 10 min pretreatment) in mouse hippocampal neurons (DIV 12–14) transduced with GFP. Filled arrowheads indicate spine growth and formation, while open arrowheads indicate spine elimination and/or reduction between the two time points. Scale bar, 10 μm. Percentage changes in dendritic spine turnover and spine volume over 10 min with different treatments are shown in *D*. Positive values indicate spine formation, while negative values indicate spine elimination between 0 and 10 min. *E*, Quantification of dendritic spine morphology in fixed neurons following HIV-1 gp120 treatment (0.5 nM for 30 min) in the absence and presence of 17αE2 (10 nM, 10 min pretreatment). *F*, Confocal images show changes in the distribution of ERα-GFP in response to 17αE2 (10 nM for 30 min) in CLU199 cells costained with DAPI for nucleus. *G*, Quantitative change of nuclear ER activation in response of HIV-1 gp120 (0.5 nM for 30 min) or 17αE2 (10 nM for 30 min) using estrogen receptor transcription factor ELISA (TransAM-ER).
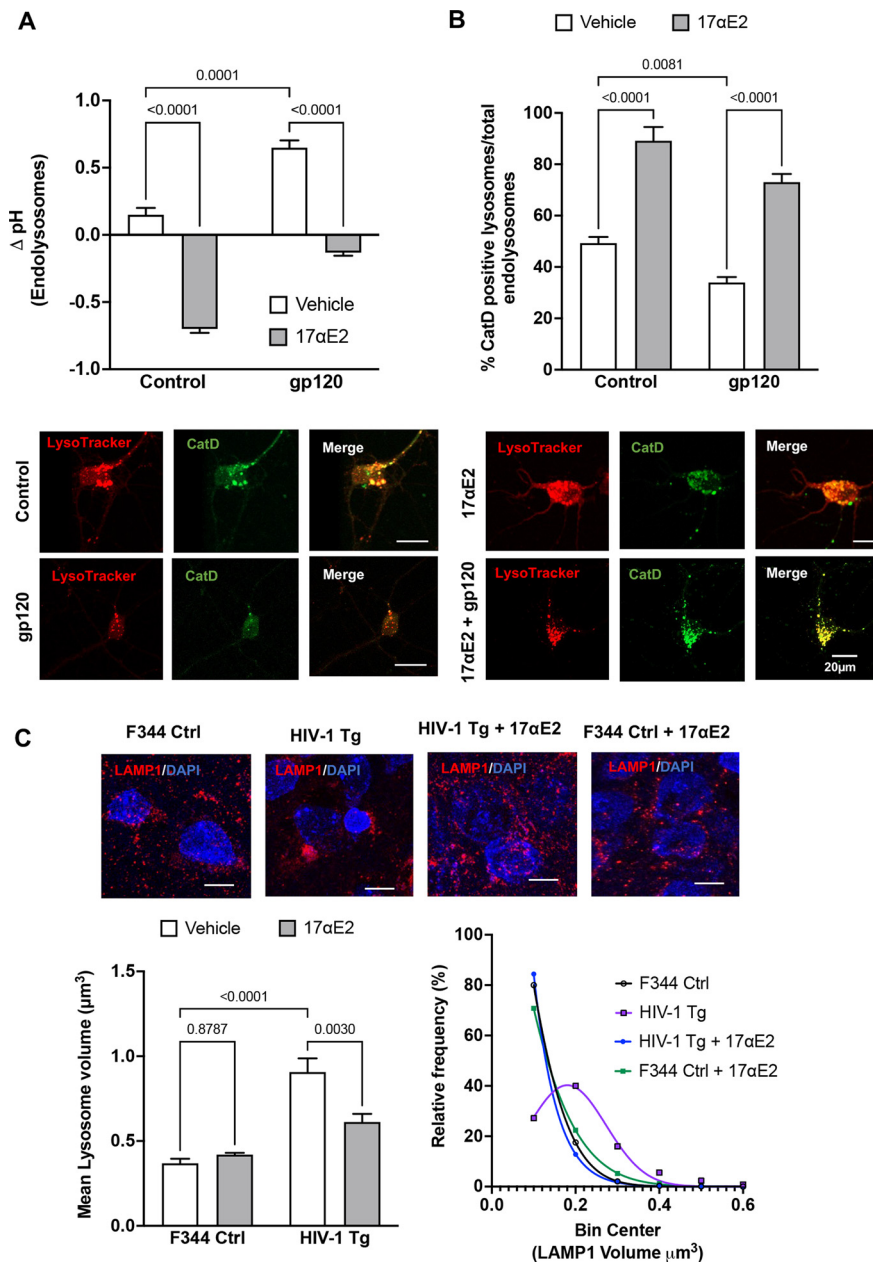
Figure 3. 17αE2 protects against HIV-1 gp120-induced endolysosome dysfunction. **A**, gp120-induced (0.5 nM for 10 min) changes in endolysosome pH in the absence and presence of 17αE2 (10 nM) in CLU199 cells. **B**, Images and quantification show gp120-induced (0.5 nM for 10 min) changes in the percentage of active CatD-positive lysosomes (as indicated by active cathepsin D staining with its fluorescent inhibitor pepstatin A-BODIPY FL versus total LysoTracker-positive endolysosomes) in the absence and presence of 17αE2 (10 nM, 10 min pretreatment). **C**, Confocal images show immunostaining of LAMP1-positive endolysosomes (red) and nuclei (DAPI; blue) in rat hippocampi (CA1). Bar graph shows that HIV-1 Tg rats exhibit increased the mean volume of LAMP1-positive endolysosomes, and this effect was significantly prevented by 17αE2. A frequency distribution plot shows that HIV-1 Tg rats exhibit higher percentage of enlarged LAMP1-positive endolysosomes, and this effect was prevented with 17αE2 treatment. At least 30 images were analyzed with 10–15 nuclei per image from five rats per group.

induced dendritic impairment do not occur through the classical genomic pathway.

17αe2 enhances endolysosome activity and protects against gp120-induced endolysosome dysfunction in neurons

The neuronal damaging effects of HIV-1 gp120 depend, at least in part, on its endocytosis and internalization (Bachis et al., 2006; Berth et al., 2015; Wenzel et al., 2017). Consistent with our published findings (Bae et al., 2014; Datta et al., 2019), we

demonstrated that HIV-1 gp120 deacidified (increased the pH) endolysosomes (Fig. 3A) and induced endolysosome dysfunction, as indicated by decreasing the percentage of active CatD-positive endolysosomes (Fig. 3B). Because neurons are long-lived postmitotic cells that require active endolysosomes to maintain neuronal homeostasis and because neurons are extraordinarily polarized cells with extensive processes that require constant vesicular membrane trafficking to establish and maintain axonal and somatodendritic plasma membrane domains, it is likely that endolysosome dysfunction, resulting from the internalization of gp120, leads to alterations in neurite morphology and dendritic spines.

Here, we determined the extent to which 17αE2 affects endolysosome function. Using fluorescent dextran-based ratiometric endolysosome pH measurement, we demonstrated that 17αE2 (10 nM for 10 min) acidified (decreases in pH) endolysosomes (Fig. 3A) and enhanced endolysosome protease activity, as evidenced by an increase in the percentage of active CatD-positive endolysosomes (Fig. 3B). Furthermore, we demonstrated that 17αE2 pretreatment (10 nM for 10 min) significantly prevented gp120-induced endolysosome deacidification (Fig. 3A) and decreased the percentage of active CatD-positive endolysosomes (Fig. 3B).

To further explore the persistent effect of 17αE2 on endolysosomes, we determined the extent to which 17αE2 affects endolysosome morphology in hippocampi of F344 control and HIV-1 Tg rats. Here, endolysosomes in hippocampal brain regions were identified by LAMP1 staining in cryostat sections of brain tissues, confocal images were reconstructed in Imaris software, and endolysosome volume were then calculated. We demonstrated that the average size of LAMP-1-positive endolysosomes was significantly increased (Fig. 3C, bar graph) and the percentage of larger endolysosomes are increased (Fig. 3C, frequency distribution curve) in HIV-1 Tg rats. Importantly, 17αE2 treatment significantly attenuated the development of enlarged endolysosome in HIV-1 Tg rats (Fig. 3C). Our findings therefore suggest that 17αE2 enhances endolysosome function and protects against gp120-induced endolysosome dysfunction. Such endolysosome-enhancing effects of 17αE2 could contribute to its modulatory effect on dendritic spines.

ERα localizes to endolysosomes

ERα has been shown to be present in vesicle like puncta localizing on early endosomes, lysosomes, and recycling endosomes
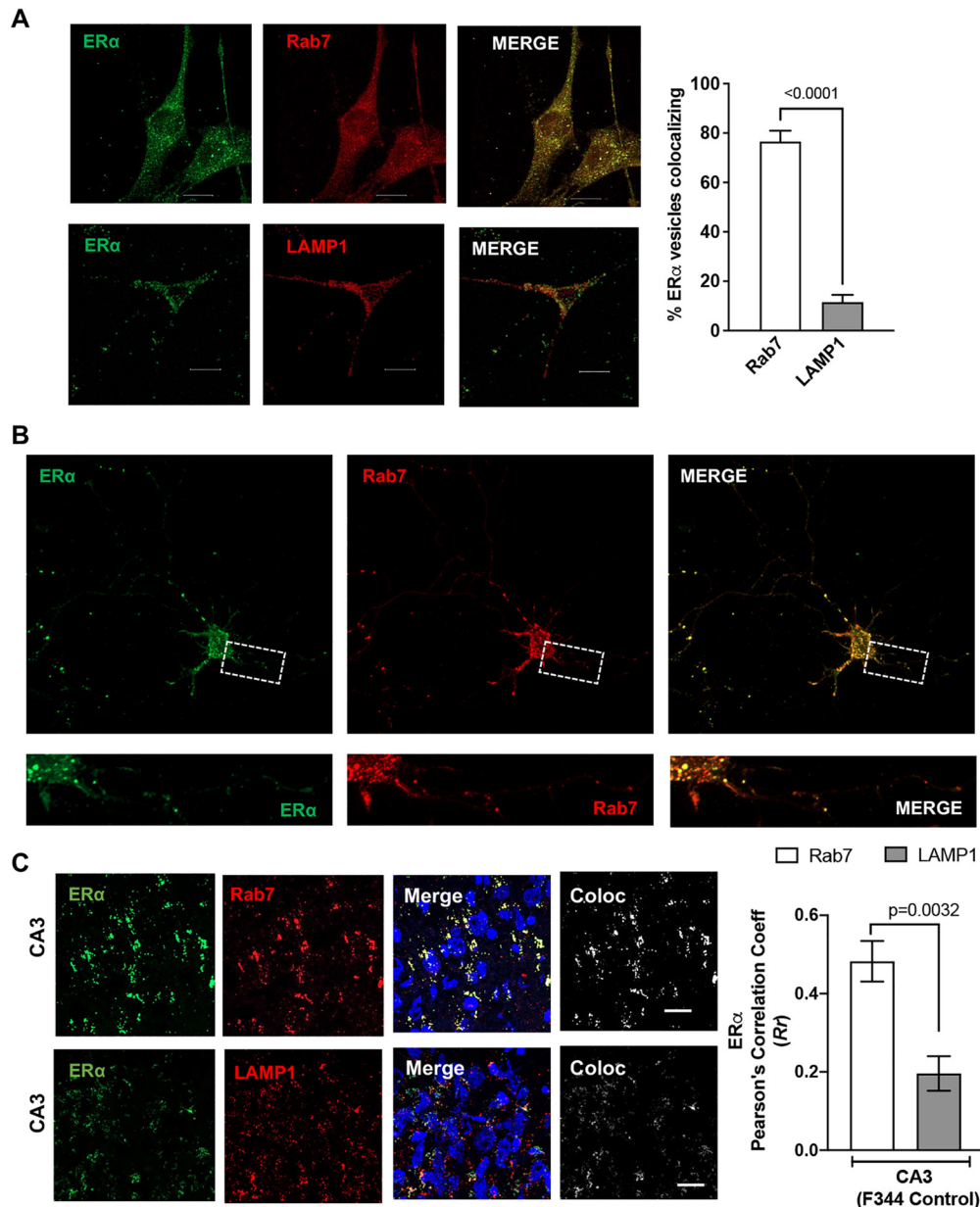
Figure 4. ERα is localized on endolysosomes. **A**, Confocal images show the codistribution of ERα (green) with Rab7 or LAMP1 in CLU199 cells. Scale bar, 10 μm. Bar graph shows the quantification of object-based colocalization by reconstructing ERα, Rab7, and LAMP1 vesicles as spots in Imaris. **B**, In primary mice hippocampal neurons (DIV 9–11), ERα (green) codistributes with Rab7 (red). Scale bar, 10 μm. **C**, Confocal images show the colocalization of ERα (green) with Rab7 or LAMP1 in CA3 hippocampal region of F344 rat (male). Scale bar, 20 μm. Bar graph shows the quantification of colocalization by Pearson's correlation coefficient. At least 30 images were analyzed with 10–15 nuclei per image from five rats per group.

(Sampayo et al., 2018). In the present study, we conducted immunolocalization studies of ERα with endolysosomes using the mouse hippocampal cell line CLU199 that is known to express both ERα and ERβ (Gingerich et al., 2010). Using object-based colocalization, which is more accurate than pixel-based colocalization for vesicular structures, we observed that ERα showed high levels (76.54 ± 4.393%) of colocalization with Rab7-positive endolysosome and to a lesser extent (14.35 ± 3.843%) with LAMP1-positive endolysosomes in both CLU199 cells and primary neurons (Fig. 4A,B, respectively). Further extending these *in vitro* findings, we determined the localization of ERα on endolysosomes using hippocampal brain sections from F344 rats. ERα similarly exhibited higher levels of colocalization with Rab7 than with LAMP1 in CA3 (Fig. 4C; Pearson's correlation coefficient (*Rr*), 0.48 ± 0.11 vs 0.29 ± 0.09). The localization of ERα on endolysosomes and our findings that 17αE2 enhances endolysosome function further pointed toward 17αE2 acting through the ERα present on Rab7- and LAMP1-positive vesicles.

ERα is involved in enhancing effects of 17αE2 on endolysosomes

The endolysosome localization of ERα has been implicated in its degradation (Sampayo et al., 2018). However, ERα being a cytosolic rather than a transmembrane protein, it can attach to the membrane via palmitoylation (Schlegel et al., 1999; Adlanmerini et al., 2014; Pedram et al., 2014). Thus, endolysosome-localized ERα most likely resides on endolysosome membrane facing the cytosol rather than facing the lumen for degradation. Given our findings that 17αE2 enhances endolysosome function, we asked whether the endolysosome-enhancing effect of 17αE2 is mediated via ERα.
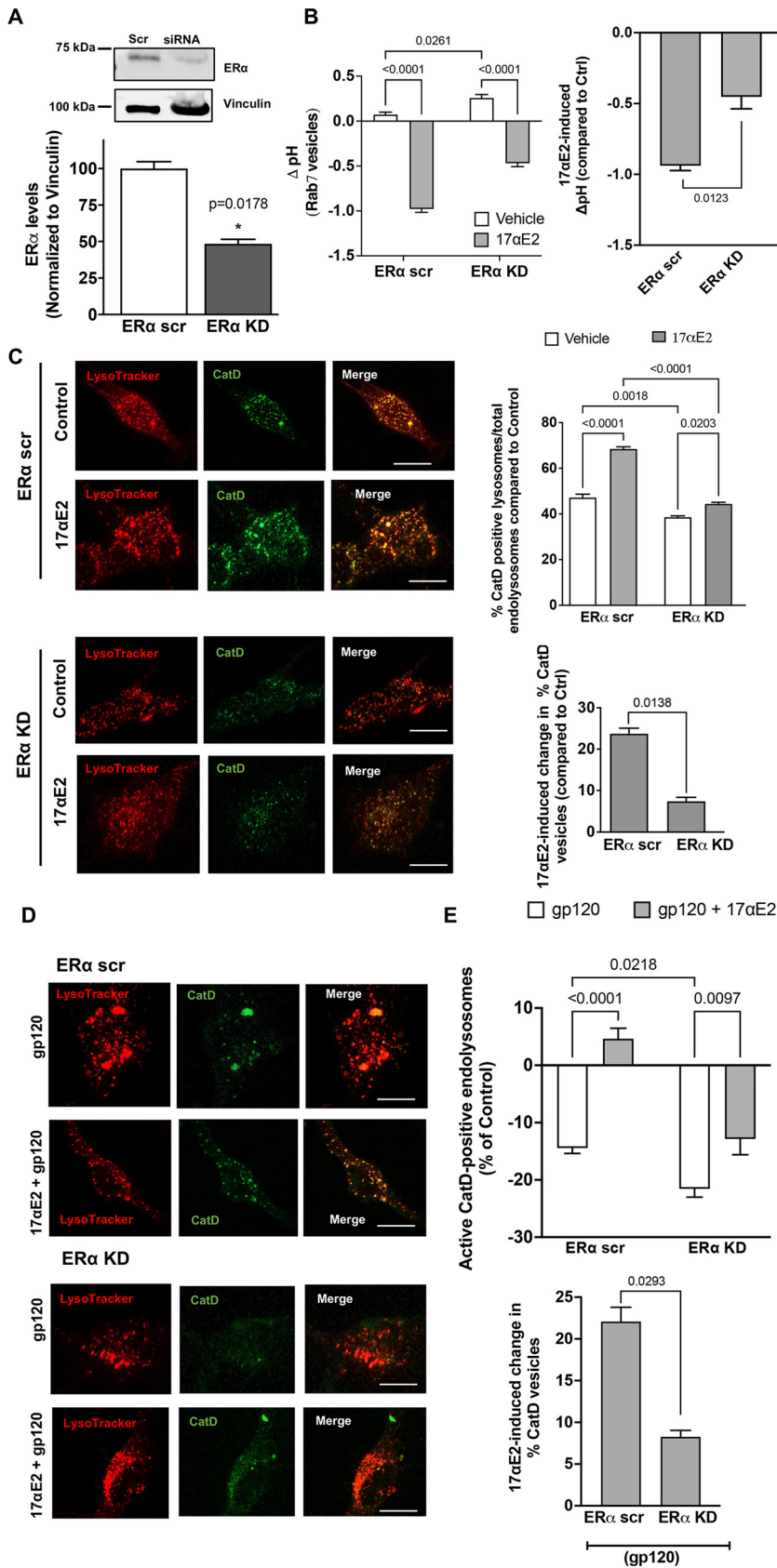
We performed siRNA-mediated knockdown of ERα in CLU199 cells and achieved 60% reduction in ERα levels (Fig. 5A). As ERα exhibits high levels of colocalization with Rab7 vesicles, we sought to further establish its role in regulating Rab7 vesicle pH. To this end, we measured the luminal pH of Rab7 vesicles instead of the total endolysosomes, by pulsing the CLU199 cells with pHrodo Dextran and Dextran Texas Red for 6 h followed by a chase of 2 h, at which point we observed the maximum incorporation of dextran in Rab7 vesicles (data not shown). To start with, the resting luminal pH of Rab7 vesicles in ERα KD cells, pH 6.59 ± 0.068, was higher than in ERα scrambled (scr) cells, pH 6.33 ± 0.067, indicating that ERα affects endolysosome pH. In ERα KD cells, 17αE2 was less able to induce Rab7 vesicle acidification (0.869 ± 0.06 U) in ERα KD cells than in ERα scr cells (1.33 ± 0.06), a difference of 0.5091 U (Fig. 5B). Thus, ERα is necessary for maintaining the optimum pH of Rab7 vesicles, where it exhibits high levels of colocalization.

To further assess endolysosome function, we determined the effect of ERα KD on lysosome hydrolase activity. We calculated active endolysosomes as the percentage of pepstatin A-BODIPLY-FL-stained cathepsin D-positive endolysosomes in total endolysosomes stained with LysoTracker Red (Fig. 5C). The percentage of active cathepsin D endolysosomes was significantly lower in ERα KD cells than in ERα scr control cells (Fig. 5C), further signifying that ERα could be responsible for maintaining endolysosome pH. In response to 17αE2 treatment, ERα KD cells failed to show the 17αE2-induced increase in the percentage of active cathepsin D endolysosomes (5.82 ± 1.29%) in ERα scr compared with ERα scr cells (21.3 ± 1.6%; Fig. 5C).

Furthermore, we determined the involvement of ERα in the protection of 17αE2 against gp120-induced endolysosome dysfunction. ERα KD further decreased gp120-induced reduction in the percentage of active

←

reduced in ERα KD cells. *C*, Confocal images and bar graph show 17αE2-induced (10 nM, 10 min pretreatment) changes in the percentage of active/mature lysosomes in ERα scr and ERα KD cells. Scale bar, 10 μm. Bottom bar graph shows that the extent of the 17αE2-induced increase in the percentage of active cathepsin D-positive endolysosomes was significantly reduced in ERα KD cells. *D*, *E*, Representative confocal images and bar graphs show that 17αE2 (10 nM, 10 min pretreatment) affects the percentage of CatD-positive active lysosomes in ERα scr and ERα KD cells treated with HIV-1 gp120 (0.5 nM, 10 min). Scale bar, 10 μm. Bottom bar graph shows the extent of 17αE2-induced restoration in HIV-1 gp120-induced decrease in the percentage of active cathepsin D-positive endolysosomes in ERα KD cells was significantly reduced.

Figure 5. ERα knockdown prevents the enhancing effects of 17αE2 on endolysosomes. *A*, Densitometric quantification of immunoblotting shows that ERα protein levels are significantly reduced with siRNA directed against ERα (ERα KD) in CLU199 cells. Vinculin is used as a loading control. *B*, 17αE2-induced (10 nM for 10 min) changes in luminal pH of Rab7-positive endolysosomes in ERα KD CLU199 cells and control cells treated with scr siRNA. The right bar graph shows that the extent of the 17αE2-induced decrease in luminal pH of Rab7-positive endolysosomes was significantly

cathepsin D endolysosomes; the percentage of cathepsin D endolysosomes decreased by 14.43 ± 2.54% in ERα scr cells compared with 21.55 ± 3.87% in ERα KD cells (Fig. 5D,E). In addition, ERα KD significantly blocked 17αE2-induced (10 nM, pretreated for 10 min) increases in the percentage of active cathepsin D endolysosomes in the presence gp120 (0.5 nM for 30 min); the ERα scr cells showed a 22.075 ± 2.964% increase in the percentage of active cathepsin D endolysosomes, whereas ERα KD cells showed an 8.264 ± 1.331% increase in the percentage of active cathepsin D endolysosomes in Figure 5, D and E. These results suggest that ERα in involved protection of 17αE2 against gp120-induced endolysosome dysfunction.

ERα is involved in protective effect of 17αE2 against gp120-induced impairment of dendritic spines

ERα has also been shown to be present in dendritic spines of glutaminergic neurons (Mukai et al., 2007), and the trafficking of lysosomes along the dendrites have been shown to correlate with synaptic AMPA-type glutamate receptors (Goo et al., 2017). Having earlier shown that ERα colocalizes largely with Rab7 vesicles, and that in primary hippocampal neurons it colocalizes with PSD-95 (which is enriched in excitatory synapses; 75.159 ± 5.34%; Fig. 6A), we sought to establish the relationship between modulation of ERα function and changes in dendritic spines. For this, we determined the involvement of ERα in the protection of 17αE2 against gp120-induced impairment of dendritic spines. We calculated the dendritic spine density in gp120-challenged (0.5 nM for 30 min) primary hippocampal neurons expressing cytosolic GFP with or without 17αE2 pretreatment (10 nM for 10 min) in both ERα scr and ERα KD cells. We were able to knock down ERα in mice primary hippocampal neurons (Fig. 6B) and as shown in Figure 6A, ERα knockdown significantly attenuated the protective effect of 17αE2 against gp120-induced reduction in dendritic spines. In ERα knock-down neurons, 17αE2 pretreatment failed to induce any significant increase in spine density in response to gp120 (0.696 ± 0.352) compared with 1.734 ± 0.729 in ERα scr control neurons, a more than twofold difference (Fig. 6C).

In primary neurons, Rab7 vesicles have been shown to be present within the dendrites, and, in addition to their importance in endolysosomal maturation (Cheng et al., 2018; Yap et al., 2018), Rab7 vesicles are also responsible for the degradation of dendritic cargo, autophagy, and neuronal growth factor signaling (Gutierrez et al., 2004; Saxena et al., 2005). Because we had already shown that ERα is primarily localized to Rab7 vesicles, we calculated the presence of Rab7 vesicles throughout the dendrites as a measure of their transport and ability to affect changes in spine turnover. To this end, ERα was knocked down with siRNA with a scrambled peptide as the control in primary hippocampal neurons (DIV 9–12) and then were stained for endogenous Rab7 and MAP2. As shown in Figure 6D, ERα knockdown reduced dendritic occupancy of Rab7 vesicles in neurons treated with gp120 (4.972 ± 1.279 and 1.432 ± 0.1258 in ERα scr and KD neurons, respectively). 17αE2 pretreatment significantly increased the Rab7 dendritic occupancy by almost three times (to 15.017 ± 1.0628) in ERα scr control neurons treated with gp120, but to only 3.222 ± 0.6428 in ERα KD neurons (Fig. 6D). These findings indicated that ERα KD affects the dendritic transport of Rab7 vesicles.

To further explore the potential consequence of ER KD and dendritic transport of Rab7 vesicles, we checked the dendritic presence of PSD-95, a postsynaptic protein that has been shown to interact with the G-protein-coupled ER receptor 1 GPR30 (Akama et al., 2013) in the dendritic spines (Akama et al., 2013)

and to regulate the trafficking of NMDA- or AMPA-type receptors to affect synaptic development and plasticity. We have also shown that ERα colocalizes with PSD-95 (Fig. 6A). Similar to the changes observed with Rab7, gp120 greatly reduced the PSD-95 dendritic occupancy in ERα KD neurons (ERα scr, 4.44 ± 1.152; ERα KD, 1.44 ± 0.345). 17αE2 pretreatment increased PSD-95 dendritic occupancy to 11.461 ± 0.5583 in ERα scr neurons, it only increased it to 2.843 ± 0.2926 with ERα KD, a difference of a factor of 4 (Fig. 6E). Together, our findings suggest that ERα is critical for the neuroprotective ability of 17αE2 against gp120-induced impairment in dendritic spines.

Endolysosome localization of ERα is responsible for the endolysosome-enhancing effect of 17αE2

S-palmitoylation of ERα (C451 in mice) has been shown to be essential for membrane localization in vivo and in various cell types (Acconcia et al., 2005; Adlanmerini et al., 2014; Pedram et al., 2014; Gustafsson et al., 2016). Here, we determined whether S-palmitoylation of ERα is involved in its endolysosome localization. Given that ERα colocalizes with Rab7-positive endolysosomes, we transfected CLU199 cells expressing Rab7-RFP with either ERα wild-type (WT)-GFP or its palmitoylation-deficient mutant ERα C451A-GFP. We observed that ERα WT-GFP was localized to discrete puncta that colocalized with Rab7-RFP. However, its palmitoylation-deficient mutant ERαC451A showed a more diffuse cytoplasmic localization with negligible Rab7 colocalization (Fig. 7A).

To further investigate whether ERα palmitoylation and localization to Rab7-positive endolysosomes are necessary for the enhancing effect of 17αE2 on endolysosomes, we compared the effect of 17αE2 on cathepsin D activity in the presence or absence of ERα palmitoylation at C451. Because we have shown that 17αE2 induces the translocation of ERα from cytosol to endolysosomes and we reason that overexpressed ERα C451A mutant will compete the binding of WT ERα to 17αE2, thus the overexpressed ERα C451A mutant will attenuate 17αE2-induced the translocation of WT ERα to endolysosomes and the enhancing effect of 17αE2 on endolysosomes. ERα-C451A mutant cells without any treatment had less than half the percentage of active cathepsin D endolysosomes compared with ERα WT (Fig. 7B). 17αE2 (10 nM for 10 min) significantly increased the percentage of cathepsin D-positive endolysosomes in ERα WT cells (by 14.283 ± 3.5%), but not in ERα C451A cells (by 10.01 ± 1.748%), a difference of 37.28% (Fig. 7B). Our findings thus indicate that endolysosome localization of ERα is responsible for the enhancing effect of 17αE2 on endolysosomes.

Endolysosomal ERα is responsible for the protective effect of 17αE2 against gp120-induced endolysosome dysfunction and impairment in dendritic spines

In our earlier experiment, we showed that membrane localization of ERα is necessary for E2-induced endolysosomal acidification (Figs. 5, 7). Because we had shown that ERα is involved in protection by 17αE2 against gp120-induced endolysosome dysfunction and impairment in dendritic spines, we next determined whether endolysosomal localization of ERα is necessary for the above effect. The difference between the 17αE2-induced increase in the percentage of CatD lysosomes between cells overexpressing ERαWT and ERαC451A was 27.88% (Fig. 8A). It therefore follows that 17αE2 fails to significantly acidify endolysosomes in ERα C451A mutant cells treated with HIV-1 gp120. Furthermore, primary hippocampal neurons expressing GFP and transfected with ERα-C451A mutant showed a significantly
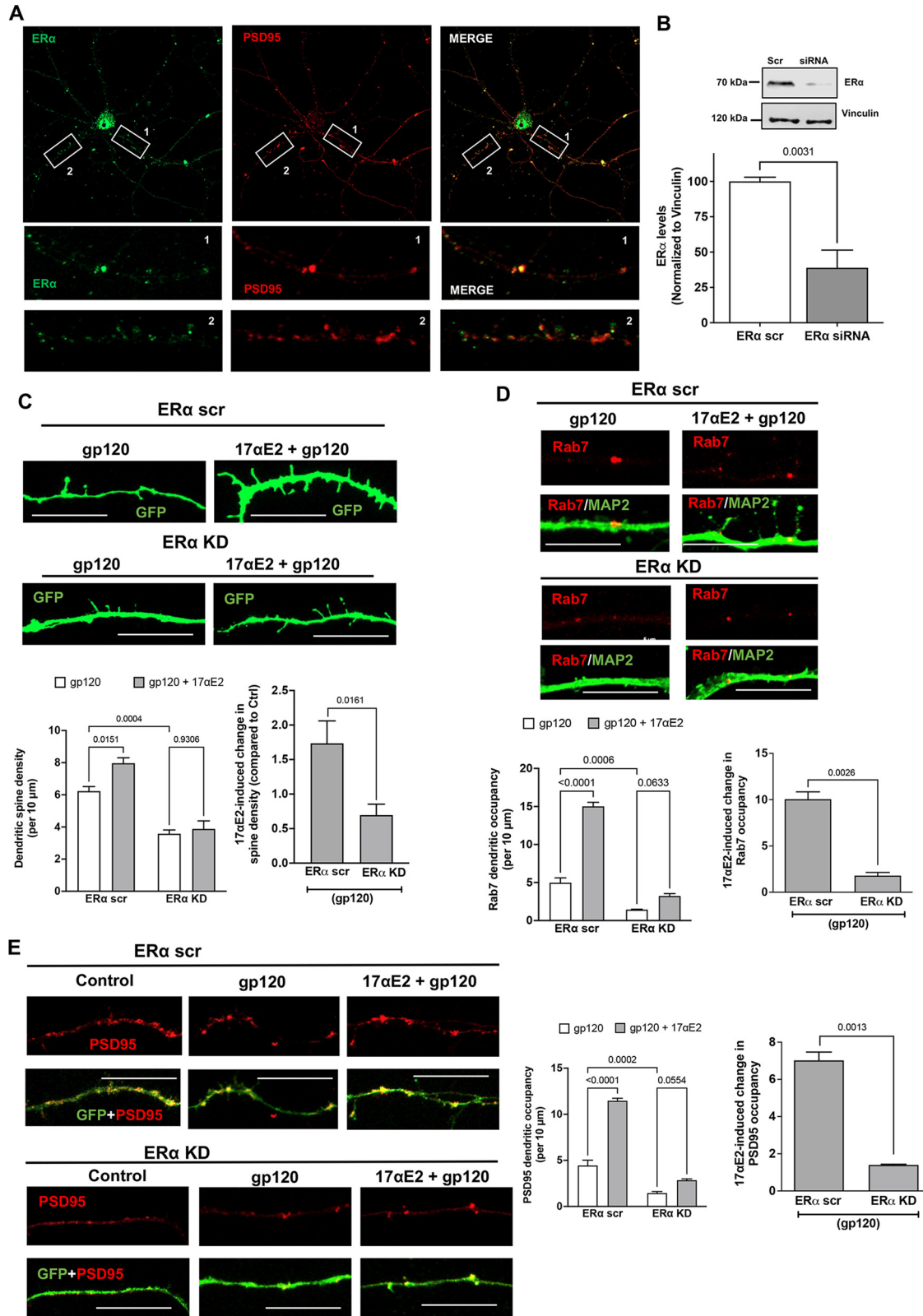
Figure 6. ERα knockdown prevents the protective effect of 17αE2 against HIV-1 gp120-induced impairment in dendritic spines. **A**, Immunostaining of ERα (green) and PSD-95 (red) in primary mouse hippocampal neurons (DIV 9–11). Colocalization of ERα and PSD-95 (75.16 ± 5.338%) along the dendrites is shown in enlarged panels. **B**, Densitometric quantification of immunoblotting show ERα protein levels in primary mouse hippocampal neurons (DIV 18) treated with ERα siRNA or scr siRNA; vinculin is used as a loading control (*n* = 4). **C**, Confocal images and bar graphs show that 17αE2 pretreatment (10 nM, 10 min) affects dendritic spine density (indicated by GFP expression) in ERα scr and ERα KD neurons (DIV 12–14) treated with HIV-1 gp120 (0.5 nM, 30 min). Bar graph on the right shows that ERα KD significantly reduced 17αE2-induced changes in spine density in gp120-treated neurons. **D**, Confocal images and bar graphs show that 17αE2 pretreatment (10 nM, 10 min) affects the occupancy of Rab-7-positive endolysosome in dendrites (identified with MAP2 staining) in ERα scr and ERα KD neurons (DIV 12–14) treated with HIV-1 gp120 (0.5 nM, 30 min). Bar graph on the right shows that ERα KD significantly reduced 17αE2-induced changes in the occupancy of Rab-7-positive endolysosome in dendrites in gp120-treated neurons. **E**, Confocal

lower dendritic spine density than ERα-WT when treated with gp120 (data not shown). Overexpressing the ERα C451A mutant also compromised the ability of 17αE2 to increase dendritic spine density in gp120-treated neurons, resulting in a difference of 5.78 (Fig. 8B). Together, our findings suggest that endolysosome localization of ERα is essential for the endolysosome-enhancing effect and neuroprotective effects of 17αE2.

Discussion

In this study, we explore the role of the endolysosome localization of ERα in endolysosome function and dendritic spines. Major findings of the present study are that endolysosome localization of ERα is not only responsible for 17αE2-induced endolysosome acidification and an increase in dendritic spines, but also for the protective effect of 17αE2 against HIV-1 gp120-induced endolysosome dysfunction and reduction in dendritic spines.

Endolysosome localization of ERα is responsible for 17αE2-induced endolysosome acidification and increases in dendritic spines

The extranuclear presence of membrane-bound ERs in neurons has been implicated in the enhancing effect of estrogen on cognition and synaptic function (Mukai et al., 2007; Hojo et al., 2008; Srivastava et al., 2011; Frick, 2015; Lai et al., 2017; Sheppard et al., 2019). These membrane-bound ERs exhibit distinct subcellular distribution patterns; ERα is mainly expressed on endolysosomes (Milner et al., 2001; Sampayo et al., 2018), ERβ is mainly mitochondrial (Yang et al., 2004; Milner et al., 2005; Liao et al., 2015), and GPER is mainly expressed on endoplasmic reticulum (Revankar et al., 2005). Activating these membrane-bound ERs could lead to the activation of multiple kinase networks, small GTPase, and prostaglandin-E2 signaling in regulating the actin dynamics governing spine plasticity (Amateau and McCarthy, 2002; Dominguez and Micevych, 2010; Christensen et al., 2011; Hasegawa et al., 2015). Although not extensively studied, 17αE2 exerts neuroprotective effects in cells

Figure 7. Endolysosome localization of ERα is responsible for the endolysosome-enhancing effects of 17αE2. *A*, Confocal images show the codistribution of ERα with Rab7-positive endolysosomes in CLU199 cells. In cells expressing wild-type ERα-GFP, the distribution of ERα WT exhibited a distinct puncta pattern, and ERα WT was localized primarily on Rab7-positive endolysosomes; however, in cells transfected with ERα palmitoylation deficit mutant (ERα C451A-GFP), ERα C451A-GFP lacked a puncta pattern, and showed a diffuse cytoplasmic localization. Scale bar, 10 μm. *B*, Confocal images and bar graphs show 17αE2-induced (10 nM for 10 min) changes in the percentage of CatD lysosomes in CLU199 cells expressing wild-type ERα (ERα WT-HA) and the ERα C451A-HA mutant that lacks endolysosome localization (ERα C451A). Scale bar, 10 μm. Bar graph at the bottom shows that the overexpressing ERα C451A mutant significantly reduced 17αE2-induced changes in the percentage of cathepsin D-positive endolysosomes.

(Green et al., 1997) and in various animal models of neuronal injury (Levin-Allerhand et al., 2002; McClean and Nuñez, 2008; Manaye et al., 2011) and promotes dendritic spine synapse formation (Luine and Frankfurt, 2012; Sengupta et al., 2019).

In brain regions such as the prefrontal cortex and hippocampus that mediate learning and memory, ERα is present in both cytoplasmic and membrane-bound fractions including the dendritic spines and at synapses (Milner et al., 2001; Hart et al., 2007; Mukai et al., 2007; Wang et al., 2010). ERα has been detected on endolysosomes in hippocampal neurons (Milner et al., 2001), and such endolysosome localization of ERα has been

←

images and bar graphs show that 17αE2 pretreatment (10 nM, 10 min) affects the occupancy of PSD-95 (red) along dendrites (GFP) in both ERα scr and ERα KD neurons (DIV 12–14) treated with HIV-1 gp120 (0.5 nM, 30 min). Bar graph on the right shows that ERα KD significantly reduced 17αE2-induced changes in the occupancy of PSD-95 in dendrites in gp120-treated neurons.
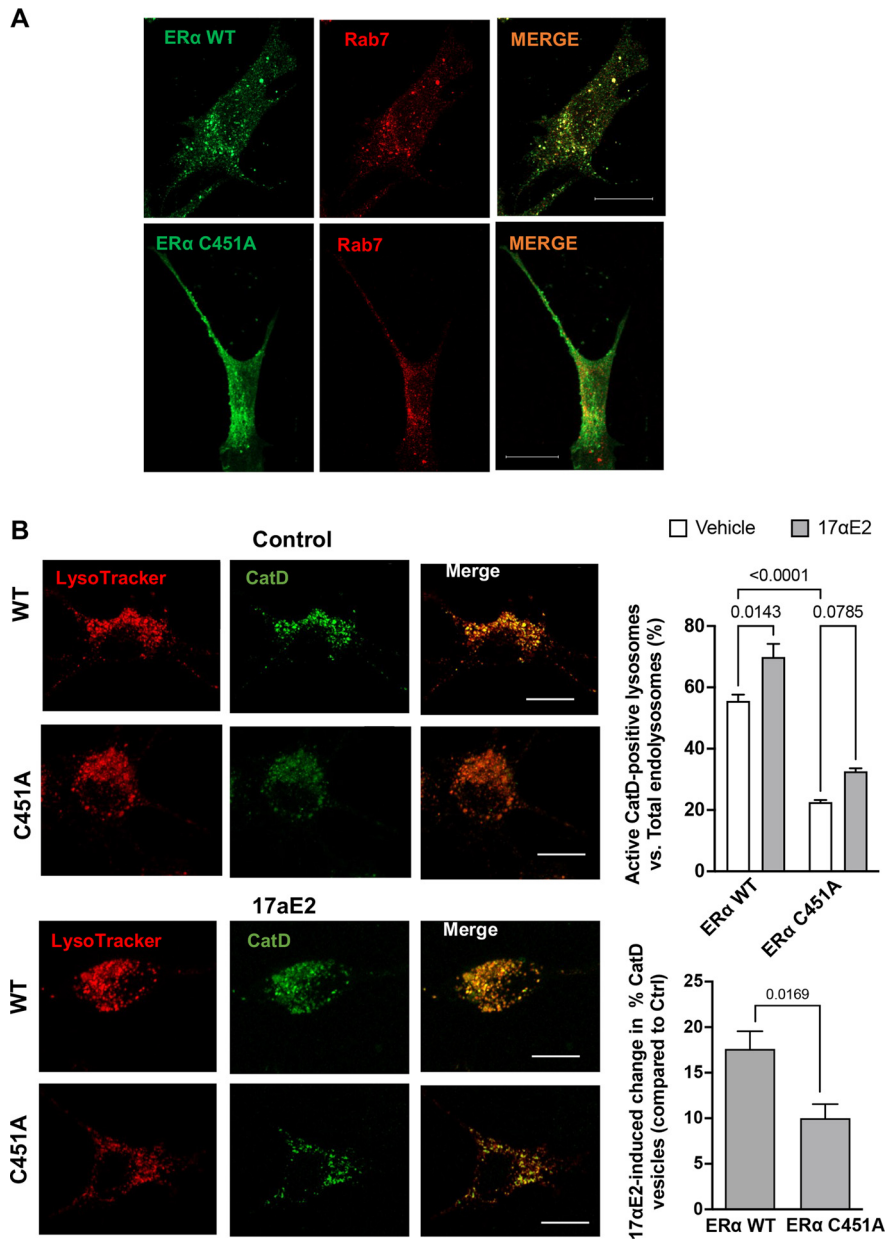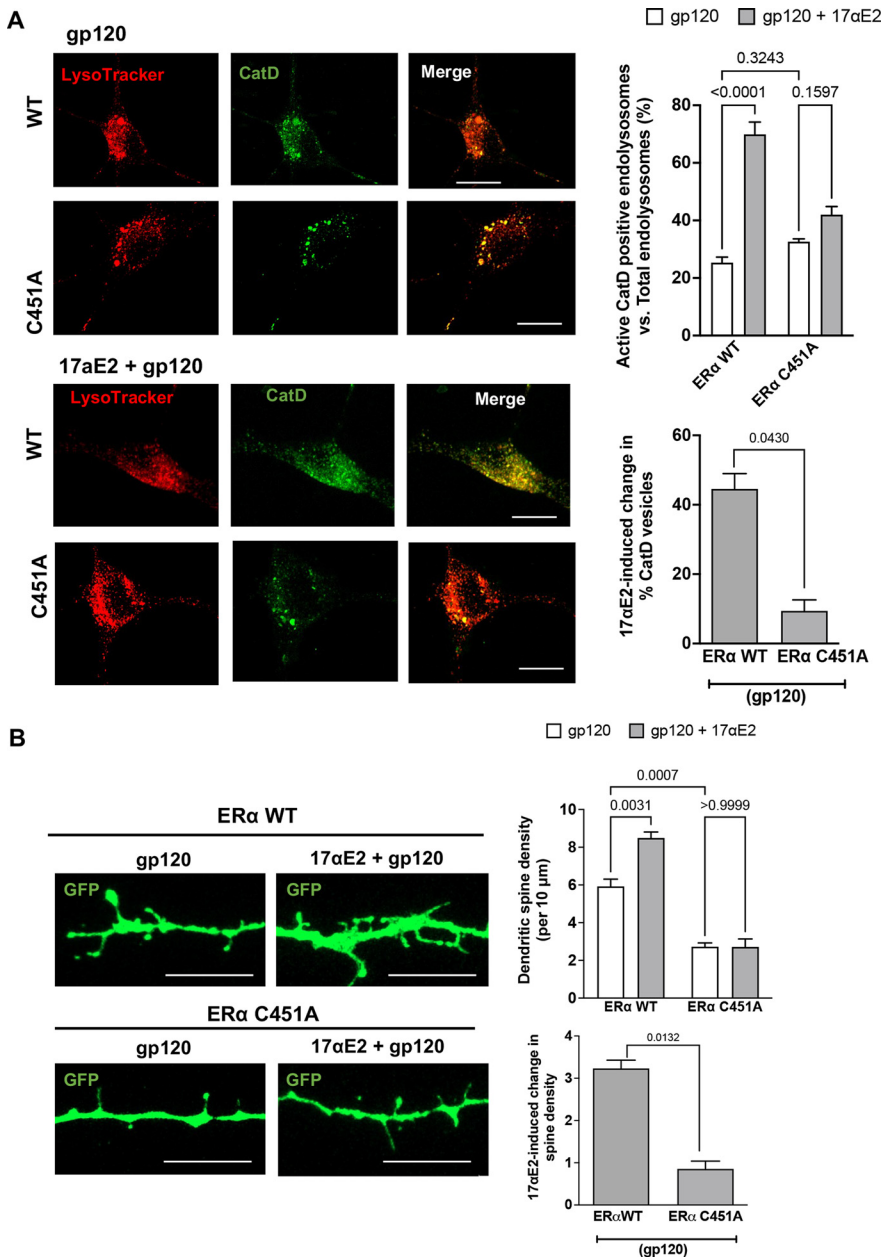
Figure 8. Endolysosome localization of ERα is responsible for the protective effect of 17αE2 against HIV-1 gp120-induced endolysosome dysfunction and reduction in dendritic spine density. **A**, Confocal images and bar graphs show that 17αE2 pretreatment (10 nM, 10 min) affects the percentage of active CatD-positive lysosomes in CLU199 cells treated with HIV-1 gp120 (0.5 nM, 30 min). Scale bar, 10 μm. Bar graph at the bottom shows that the overexpressing ERα C451A mutant significantly reduced 17αE2-induced changes in the percentage of cathepsin D-positive endolysosomes in CLU199 cells treated with HIV-1 gp120. **B**, Confocal images and bar graphs show that 17αE2 pretreatment (10 nM, 10 min) affects dendritic spine density (indicated by GFP expression) in both ERα WT and ERα C451A neurons treated with HIV-1 gp120 (0.5 nM, 30 min). Scale bar, 10 μm. Bar graph at the bottom shows that the overexpressing ERα C451A mutant significantly reduced 17αE2-induced changes in dendritic spine density in neurons treated with HIV-1 gp120.

that membrane-permeable 17αE2 activates endolysosome-localized ERα and initiates an endolysosome-dependent action of 17αE2.

We therefore investigated whether endolysosome localization of ERα could have a direct effect on endolysosome function. Indeed, our findings demonstrate clearly that endolysosome localization of ERα is responsible for 17αE2-induced endolysosome acidification in neurons. First, ERα is present on endolysosomes in neurons. Second, 17αE2 acidifies endolysosomes and enhances endolysosome function. Third, ERα knockdown prevents the ability of 17αE2 to acidify endolysosomes. Fourth, Overexpressing an ERα mutant (C451A) that is deficient in the known palmitoylation site (Adlanmerini et al., 2014; Pedram et al., 2014) and lacks endolysosome localization prevents 17αE2-induced enhancement of endolysosome function. The underlying mechanisms by which 17αE2 acts on endolysosome-localized ERα to acidify endolysosomes remains to be further investigated.

Endolysosomes have been shown to modulate synaptic plasticity through the dendritic spines (Goo et al., 2017; Padamsey et al., 2017; Cheng et al., 2018; Yap et al., 2018). Given our findings that endolysosome-localized ERα is responsible for 17αE2-induced endolysosome acidification in neurons, and that 17αE2 increases dendritic spine density, we further investigated the involvement of endolysosomal ERα in 17αE2-induced enhancing effects on dendritic spines. Our findings demonstrate clearly that endolysosomal ERα is responsible for 17αE2-induced enhancing effects on dendritic spines; either ERα knockdown or overexpressing the ERα mutant (C451A) that lacks endolysosome localization prevents the ability of 17αE2 to increase dendritic spine density.

Being at the crossroads of transporting membrane and membrane proteins to synapses and dendritic spines and in the degradation of dendritic cargos, endolysosomes play an

implicated in its degradation (Totta et al., 2014; Sampayo et al., 2018). However, ERα is not a transmembrane protein, and as a cytosolic protein ERα can be attached to the membrane via palmitoylation (Schlegel et al., 1999; Adlanmerini et al., 2014; Pedram et al., 2014). It has been shown that 30 min of estradiol treatment increase ERα levels along the endocytic pathway (Norfleet et al., 1999; Dominguez and Micevych, 2010; Christensen and Micevych, 2012). This endolysosome-localized ERα most likely resides on endolysosome membrane facing the cytosol rather than facing lumen for degradation. It is more likely

important role in the modulating of dendritic spine and synaptic plasticity (Goo et al., 2017; Padamsey et al., 2017; Nikoletopoulou and Tavernarakis, 2018; Yap et al., 2018). We speculate that 17αE2-induced endolysosome acidification could affect the degradative capacity and motility of these endolysosomes traveling along dendrites (Tsuruta and Dolmetsch, 2015), thus regulating dendritic spine remodeling. Our findings show that 17αE2 increases dendritic occupancy of ERα carrying Rab7-positive endolysosomes, an effect that is blocked by ERα knockdown.

Rab7 also controls the trafficking of multiple axonal and dendritic cargoes including TrkA, Nsg1, and Nsg2 (Saxena et al., 2005; Yap et al., 2018), and, because of the considerable overlap between Rab7 and LAMP1 endolysosomal markers, 17αE2 induced changes in both the dendritic occupancy of Rab7-LAMP1 vesicles as well as in their degradative capacity (measured by cathepsin D activity) could potentially determine the local hydrolase activity of the lysosomes in modulating spine turnover. In addition to colocalization with Rab7-postive late endosomes along the dendrites, ERα also colocalizes partially with PSD-95, which has earlier been shown to interact with another ER, the GPR30 (Akama et al., 2013). Therefore, we also show that 17αE2 increases dendritic occupancy of PSD-95 puncta, an effect that is blocked by ERα knockdown. Thus, endolysosomal ERα could affect PSD-95 trafficking in dendrites (Yoo et al., 2019), modulating synaptic plasticity. Additionally, endolysosomal ERα could also regulate dendritic spine remodeling by affecting lysosomal exocytosis and the subsequent action of matrix metallopeptidase 9 (Michaluk et al., 2011; Padamsey et al., 2017). Nonetheless, detailed mechanisms whereby endolysosome localization of ERα modulates dendritic spines warrants further investigation.

Endolysosomal localization of ERα is responsible for protective effect of 17αE2 against HIV-1 gp120-induced endolysosome dysfunction and reduction in dendritic spines

Endolysosome dysfunction, which represents a central event in a wide range of age-related neurodegenerative disorders (Nixon, 2013, 2020; Bonam et al., 2019), has been implicated in HIV-1-infected individuals with HAND (Gelman et al., 2005; Spector and Zhou, 2008; Zhou and Spector, 2008; Cysique et al., 2015). We and others have shown that HIV-1 and various HIV-1 viral-related factors (viral proteins and ART drugs) have been shown to disrupt endolysosomal structure and function. Here, we also demonstrate that endolysosomes are enlarged in hippocampal brain regions from the HIV-1 Tg rat, a model that closely resembles neurocognitive impairments of HIV-1-positive individuals (Reid et al., 2001; Royal et al., 2012).

We demonstrated that 17αE2 protects against gp120-induced alteration in dendritic spines in primary neurons and in HIV-1 Tg rats. HIV-1 gp120 contributes to neuronal injury through both direct and indirect mechanisms. The direct neuronal damaging effects of HIV-1 gp120 depend, in part, on its endocytosis and internalization (Bachis et al., 2006; Berth et al., 2015; Wenzel et al., 2017). Here, we further demonstrated the association between gp120-induced endolysosome dysfunction and gp120-induced reduction in dendritic spines and the association between endolysosome enlargement and reduction in dendritic spines in HIV-1 Tg rats, indicating that endolysosome dysfunction could lead to reduction in dendritic spines. While the present study is constrained by the simplicity of using only gp120 *in vitro* compared with the HIV-1 Tg rat model that expresses many other viral proteins, including other neurotoxic proteins such as Tat and Nef, we had shown that both HIV-1 Tat and gp120 are endocytosed and deacidify the endolysosomes (Hui et al., 2012; Datta et al., 2019; Halcrow et al., 2021), implying that there could be a significant degree of overlap between their mechanistic actions.

Based on our findings that endolysosomal localization of ERα is important for 17αE2-induced enhancement of endolysosome function and an increase in dendritic spine density, we further determined the involvement of endolysosome localization of ERα in protective effect of 17αE2 on gp120-induced endolysosome dysfunction and synaptodendritic impairment. We demonstrated that either ERα knockdown or overexpressing the palmitoylation-deficient ERα mutant (C451A) that lacks endolysosome localization prevents the ability of 17αE2 to protect against gp120-induced endolysosome dysfunction and synaptodendritic impairment. These findings suggest that gp120-induced endolysosome dysfunction could lead to a reduction in dendritic spines. Mechanistically, gp120-induced endolysosomal deacidification could result in impaired proteolysis and defective trafficking of Rab7-positive endolysosomes and PSD-95-positive vesicles along dendrites, which could then lead to reduced dendritic spines and synaptic disruption, and these gp120-induced effects can be prevented by the activation of endolysosome-localized ERα by 17αE2. Our studies therefore show that 17αE2 is capable of mitigating some of the direct synaptodendritic damaging effects of HIV-1 gp120; however, further detailed mechanistic studies are needed to determine whether and how these different pathways interact.

In summary, findings from the present study demonstrate clearly that endolysosome localization of ERα is responsible not only for 17αE2-induced endolysosome acidification and an increase in dendritic spines, but also for the protective effect of 17αE2 against HIV-1 gp120-induced endolysosome dysfunction and reduction in dendritic spines. Given the physical and functional compartmentalization of different neuronal compartments coupled with the complexity of dendritic spine plasticity in the highly polarized neurons, this study is not without its caveats (e. g., brain levels of 17αE2 were not measured), but nevertheless provides novel mechanistic insights into the neuroprotective effect of 17αE2 and may lead to the development of novel therapeutic strategies against HAND.

References

Acconcia F, Ascenzi P, Bocedi A, Spisni E, Tomasi V, Trentalance A, Visca P, Marino M (2005) Palmitoylation-dependent estrogen receptor alpha membrane localization: regulation by 17β-estradiol. Mol Biol Cell 16:231–237.

Adlanmerini M, Solinhac R, Abot A, Fabre A, Raymond-Letron I, Guihot AL, Boudou F, Sautier L, Vessières E, Kim SH, Lière P, Fontaine C, Krust A, Chambon P, Katzenellenbogen JA, Gourdy P, Shaul PW, Henrion D, Arnal JF, Lenfant F (2014) Mutation of the palmitoylation site of estrogen receptor α in vivo reveals tissue-specific roles for membrane versus nuclear actions. Proc Natl Acad Sci U S A 111:E283–E290.

Akama KT, Thompson LI, Milner TA, McEwen BS (2013) Post-synaptic density-95 (PSD-95) binding capacity of G-protein-coupled receptor 30 (GPR30), an estrogen receptor that can be identified in hippocampal dendritic spines. J Biol Chem 288:6438–6450.

Alford K, Vera JH (2018) Cognitive Impairment in people living with HIV in the ART era: a review. Br Med Bull 127:55–68.

Amateau SK, McCarthy MM (2002) A novel mechanism of dendritic spine plasticity involving estradiol induction of prostaglandin-E2. J Neurosci 22:8586–8596.

Bachis A, Aden SA, Nosheny RL, Andrews PM, Mocchetti I (2006) Axonal transport of human immunodeficiency virus type 1 envelope protein glycoprotein 120 is found in association with neuronal apoptosis. J Neurosci 26:6771–6780.

Bae M, Patel N, Xu H, Lee M, Tominaga-Yamanaka K, Nath A, Geiger J, Gorospe M, Mattson MP, Haughey NJ (2014) Activation of TRPML1 clears intraneuronal Aβ in preclinical models of HIV infection. J Neurosci 34:11485–11503.

Bassuk SS, Manson JE (2016) The timing hypothesis: do coronary risks of menopausal hormone therapy vary by age or time since menopause onset? Metabolism 65:794–803.

Berth S, Caicedo HH, Sarma T, Morfini G, Brady ST (2015) Internalization and axonal transport of the HIV glycoprotein gp120. ASN Neuro 7:175909141456818.

Bertrand SJ, Mactutus CF, Aksenova MV, Espensen-Sturges TD, Booze RM (2014) Synaptodendritic recovery following HIV Tat exposure: neurorestoration by phytoestrogens. J Neurochem 128:140–151.

Bhaskaran K, Mussini C, Antinori A, Walker AS, Dorrucci M, Sabin C, Phillips A, Porter K (2008) Changes in the incidence and predictors of human immunodeficiency virus-associated dementia in the era of highly active antiretroviral therapy. Ann Neurol 63:213–221.

Bonam SR, Wang F, Muller S (2019) Lysosomes as a therapeutic target. Nat Rev Drug Discov 18:923–948.

Bruce-Keller AJ, Barger SW, Moss NI, Pham JT, Keller JN, Nath A (2001) Pro-inflammatory and pro-oxidant properties of the HIV protein Tat in a microglial cell line: attenuation by 17 beta-estradiol. J Neurochem 78:1315–1324.

Campbell GR, Rawat P, Bruckman RS, Spector SA (2015) Human immunodeficiency virus type 1 Nef inhibits autophagy through transcription factor EB sequestration. PLoS Pathog 11:e1005018.

Chen X, Hui L, Geiger NH, Haughey NJ, Geiger JD (2013) Endolysosome involvement in HIV-1 transactivator protein-induced neuronal amyloid beta production. Neurobiol Aging 34:2370–2378.

Cheng XT, Xie YX, Zhou B, Huang N, Farfel-Becker T, Sheng ZH (2018) Characterization of LAMP1-labeled nondegradative lysosomal and endocytic compartments in neurons. J Cell Biol 217:3127–3139.

Christensen A, Micevych P (2012) CAV1 siRNA reduces membrane estrogen receptor-α levels and attenuates sexual receptivity. Endocrinology 153:3872–3877.

Christensen A, Dewing P, Micevych P (2011) Membrane-initiated estradiol signaling induces spinogenesis required for female sexual receptivity. J Neurosci 31:17583–17589.

Cinti A, Le Sage V, Milev MP, Valiente-Echeverría F, Crossie C, Miron M-J, Panté N, Olivier M, Mouland AJ (2017) HIV-1 enhances mTORC1 activity and repositions lysosomes to the periphery by co-opting Rag GTPases. Sci Rep 7:5515.

Corasaniti MT, Amantea D, Russo R, Piccirilli S, Leta A, Corazzari M, Nappi G, Bagetta G (2005) 17beta-estradiol reduces neuronal apoptosis induced by HIV-1 gp120 in the neocortex of rat. Neurotoxicology 26:893–903.

Cushman M, Larson JC, Rosendaal FR, Heckbert SR, Curb JD, Phillips LS, Baird AE, Eaton CB, Stafford RS (2018) Biomarkers, menopausal hormone therapy and risk of venous thrombosis: the Women's Health Initiative. Res Pract Thromb Haemost 2:310–319.

Cysique LA, Hewitt T, Croitoru-Lamoury J, Taddei K, Martins RN, Chew CS, Davies NN, Price P, Brew BJ (2015) APOE epsilon4 moderates abnormal CSF-abeta-42 levels, while neurocognitive impairment is associated with abnormal CSF tau levels in HIV+ individuals - a cross-sectional observational study. BMC Neurol 15:51.

Dagur RS, New-Aaron M, Ganesan M, Wang W, Romanova S, Kidambi S, Kharbanda KK, Poluektova LY, Osna NA (2021) Alcohol-and-HIV-induced lysosomal dysfunction regulates extracellular vesicles secretion in vitro and in liver-humanized mice. Biology (Basel) 10:29.

D'Alonzo M, Bounous VE, Villa M, Biglia N (2019) Current evidence of the oncological benefit-risk profile of hormone replacement therapy. Medicina (Kaunas) 55:573.

Datta G, Miller NM, Afghah Z, Geiger JD, Chen X (2019) HIV-1 gp120 promotes lysosomal exocytosis in human Schwann cells. Front Cell Neurosci 13:329.

Dominguez R, Micevych P (2010) Estradiol rapidly regulates membrane estrogen receptor alpha levels in hypothalamic neurons. J Neurosci 30:12589–12596.

Du F (2019) Golgi-Cox staining of neuronal dendrites and dendritic spines with FD Rapid GolgiStain™ Kit. Curr Protoc Neurosci 88:e69.

Ellis R, Langford D, Masliah E (2007) HIV and antiretroviral therapy in the brain: neuronal injury and repair. Nat Rev Neurosci 8:33–44.

Everall I, Heaton R, Marcotte T, Ellis R, McCutchan J, Atkinson J, Grant I, Mallory M, Masliah E (1999) Cortical synaptic density is reduced in mild to moderate human immunodeficiency virus neurocognitive disorder. HNRC Group. HIV Neurobehavioral Research Center. Brain Pathol 9:209–217.

Festa L, Gutoskey CJ, Graziano A, Waterhouse BD, Meucci O (2015) Induction of interleukin-1β by human immunodeficiency virus-1 viral proteins leads to increased levels of neuronal ferritin heavy chain, synaptic injury, and deficits in flexible attention. J Neurosci 35:10550–10561.

Fields J, Dumaop W, Eleuteri S, Elueteri S, Campos S, Serger E, Trejo M, Kosberg K, Adame A, Spencer B, Rockenstein E, He JJ, Masliah E (2015)

HIV-1 Tat alters neuronal autophagy by modulating autophagosome fusion to the lysosome: implications for HIV-associated neurocognitive disorders. J Neurosci 35:1921–1938.

Frick KM (2015) Molecular mechanisms underlying the memory-enhancing effects of estradiol. Horm Behav 74:4–18.

Garratt M, Bower B, Garcia GG, Miller RA (2017) Sex differences in lifespan extension with acarbose and 17-α estradiol: gonadal hormones underlie male-specific improvements in glucose tolerance and mTORC2 signaling. Aging Cell 16:1256–1266.

Gelman BB, Soukup VM, Holzer CE 3rd, Fabian RH, Schuenke KW, Keherly MJ, Richey FJ, Lahart CJ (2005) Potential role for white matter lysosome expansion in HIV-associated dementia. J Acquir Immune Defic Syndr 39:422–425.

Gingerich S, Kim GL, Chalmers JA, Koletar MM, Wang X, Wang Y, Belsham DD (2010) Estrogen receptor α and G-protein coupled receptor 30 mediate the neuroprotective effects of 17β-estradiol in novel murine hippocampal cell models. Neuroscience 170:54–66.

Gonzalez-Scarano F, Martin-Garcia J (2005) The neuropathogenesis of AIDS. Nat Rev Immunol 5:69–81.

Goo MS, Sancho L, Slepak N, Boassa D, Deerinck TJ, Ellisman MH, Bloodgood BL, Patrick GN (2017) Activity-dependent trafficking of lysosomes in dendrites and dendritic spines. J Cell Biol 216:2499–2513.

Grant I, Franklin DR, Deutsch R, Woods SP, Vaida F, Ellis RJ, Letendre SL, Marcotte TD, Atkinson JH, Collier AC, Marra CM, Clifford DB, Gelman BB, McArthur JC, Morgello S, Simpson DM, McCutchan JA, Abramson I, Gamst A, Fennema-Notestine C, et al. (2014) Asymptomatic HIV-associated neurocognitive impairment increases risk for symptomatic decline. Neurology 82:2055–2062.

Green PS, Bishop J, Simpkins JW (1997) 17α-Estradiol exerts neuroprotective effects on SK-N-SH cells. J Neurosci 17:511–515.

Gustafsson KL, Farman H, Henning P, Lionikaite V, Movérare-Skrtic S, Wu J, Ryberg H, Koskela A, Gustafsson JA, Tuukkanen J, Levin ER, Ohlsson C, Lagerquist MK (2016) The role of membrane ERα signaling in bone and other major estrogen responsive tissues. Sci Rep 6:29473.

Gutierrez MG, Munafó DB, Berón W, Colombo MI (2004) Rab7 is required for the normal progression of the autophagic pathway in mammalian cells. J Cell Sci 117:2687–2697.

Halcrow PW, Lakpa KL, Khan N, Afghah Z, Miller N, Datta G, Chen X, Geiger JD (2021) HIV-1 gp120-induced endolysosome de-acidification leads to efflux of endolysosome iron, and increases in mitochondrial iron and reactive oxygen species. J Neuroimmune Pharmacol. Advance online publication. Retrieved April 8, 2021. doi: 10.1007/s11481-021-09995-2.

Hall HI, Song R, Rhodes P, Prejean J, An Q, Lee LM, Karon J, Brookmeyer R, Kaplan EH, McKenna MT, Janssen RS (2008) Estimation of HIV incidence in the United States. JAMA 300:520–529.

Harrison DE, Strong R, Allison DB, Ames BN, Astle CM, Atamna H, Fernandez E, Flurkey K, Javors MA, Nadon NL, Nelson JF, Pletcher S, Simpkins JW, Smith D, Wilkinson JE, Miller RA (2014) Acarbose, 17-α-estradiol, and nordihydroguaiaretic acid extend mouse lifespan preferentially in males. Aging Cell 13:273–282.

Harrison DE, Strong R, Reifsnyder P, Kumar N, Fernandez E, Flurkey K, Javors MA, Lopez-Cruzan M, Macchiarini F, Nelson JF, Bitto A, Sindler AL, Cortopassi G, Kavanagh K, Leng L, Bucala R, Rosenthal N, Salmon A, Stearns TM, Bogue M, et al. (2021) 17-a-estradiol late in life extends lifespan in aging UM-HET3 male mice; nicotinamide riboside and three other drugs do not affect lifespan in either sex. Aging Cell 20:e13328.

Hart SA, Snyder MA, Smejkalova T, Woolley CS (2007) Estrogen mobilizes a subset of estrogen receptor-α-immunoreactive vesicles in inhibitory presynaptic boutons in hippocampal CA1. J Neurosci 27:2102–2111.

Hasegawa Y, Hojo Y, Kojima H, Ikeda M, Hotta K, Sato R, Ooishi Y, Yoshiya M, Chung BC, Yamazaki T, Kawato S (2015) Estradiol rapidly modulates synaptic plasticity of hippocampal neurons: involvement of kinase networks. Brain Res 1621:147–161.

Henderson LJ, Johnson TP, Smith BR, Reoma LB, Santamaria UA, Bachani M, Demarino C, Barclay RA, Snow J, Sacktor N, McArthur J, Letendre S, Steiner J, Kashanchi F, Nath A (2019) Presence of Tat and transactivation response element in spinal fluid despite antiretroviral therapy. AIDS 33 [Suppl 2]:S145–S157.

Heron PM, Turchan-Cholewo J, Bruce-Keller AJ, Wilson ME (2009) Estrogen receptor alpha inhibits the estrogen-mediated suppression of HIV transcription in astrocytes: implications for estrogen neuroprotection in HIV dementia. AIDS Res Hum Retroviruses 25:1071–1081.

Hojo Y, Murakami G, Mukai H, Higo S, Hatanaka Y, Ogiue-Ikeda M, Ishii H, Kimoto T, Kawato S (2008) Estrogen synthesis in the brain–role in synaptic plasticity and memory. Mol Cell Endocrinol 290:31–43.

Howells P, Modarres M, Samuel M, Taylor C, Hamoda H (2019) Experience of hormone replacement therapy in postmenopausal women living with HIV. Post Reprod Health 25:80–85.

Hui L, Chen X, Haughey NJ, Geiger JD (2012) Role of endolysosomes in HIV-1 Tat-induced neurotoxicity. ASN Neuro 4:243–252.

Hui L, Ye Y, Soliman ML, Lakpa KL, Miller NM, Afghah Z, Geiger JD, Chen X (2021) Antiretroviral drugs promote amyloidogenesis by de-acidifying endolysosomes. J Neuroimmune Pharmacol 16:159–168.

Ikeda T, Makino Y, Yamada MK (2015) 17α-estradiol is generated locally in the male rat brain and can regulate GAD65 expression and anxiety. Neuropharmacology 90:9–14.

Johnson TP, Patel K, Johnson KR, Maric D, Calabresi PA, Hasbun R, Nath A (2013) Induction of IL-17 and nonclassical T-cell activation by HIV-Tat protein. Proc Natl Acad Sci U S A 110:13588–13593.

Keys B, Karis J, Fadeel B, Valentin A, Norkrans G, Hagberg L, Chiodi F (1993) V3 sequences of paired HIV-1 isolates from blood and cerebrospinal fluid cluster according to host and show variation related to the clinical stage of disease. Virology 196:475–483.

Klasse PJ, Moore JP (2004) Is there enough gp120 in the body fluids of HIV-1-infected individuals to have biologically significant effects? Virology 323:1–8.

Kovacs JM, Nkolola JP, Peng H, Cheung A, Perry J, Miller CA, Seaman MS, Barouch DH, Chen B (2012) HIV-1 envelope trimer elicits more potent neutralizing antibody responses than monomeric gp120. Proc Natl Acad Sci U S A 109:12111–12116.

Lai YJ, Yu D, Zhang JH, Chen GJ (2017) Cooperation of genomic and rapid nongenomic actions of estrogens in synaptic plasticity. Mol Neurobiol 54:4113–4126.

Levin-Allerhand JA, Lominska CE, Wang J, Smith JD (2002) 17α-estradiol and 17β-estradiol treatments are effective in lowering cerebral amyloid-β levels in AβPPSWE transgenic mice. J Alzheimers Dis 4:449–457.

Li C, Brake WG, Romeo RD, Dunlop JC, Gordon M, Buzescu R, Magarinos AM, Allen PB, Greengard P, Luine V, McEwen BS (2004) Estrogen alters hippocampal dendritic spine shape and enhances synaptic protein immunoreactivity and spatial memory in female mice. Proc Natl Acad Sci U S A 101:2185–2190.

Liao TL, Tzeng CR, Yu CL, Wang YP, Kao SH (2015) Estrogen receptor-β in mitochondria: implications for mitochondrial bioenergetics and tumorigenesis. Ann N Y Acad Sci 1350:52–60.

Luine VN, Frankfurt M (2012) Estrogens facilitate memory processing through membrane mediated mechanisms and alterations in spine density. Front Neuroendocrinol 33:388–402.

Maki PM, Springer G, Anastos K, Gustafson DR, Weber K, Vance D, Dykxhoorn D, Milam J, Adimora AA, Kassaye SG, Waldrop D, Rubin LH (2021) Cognitive changes during the menopausal transition: a longitudinal study in women with and without HIV. Menopause 28:360–368.

Manaye KF, Allard JS, Kalifa S, Drew AC, Xu G, Ingram DK, de Cabo R, Mouton PR (2011) 17α-estradiol attenuates neuron loss in ovariectomized Dtg AβPP/PS1 mice. J Alzheimers Dis 23:629–639.

Maschke M, Kastrup O, Esser S, Ross B, Hengge U, Hufnagel A (2000) Incidence and prevalence of neurological disorders associated with HIV since the introduction of highly active antiretroviral therapy (HAART). J Neurol Neurosurg Psychiatry 69:376–380.

Masliah E, Ellis RJ, Mallory M, Heaton RK, Marcotte TD, Nelson JA, Grant I, Atkinson JH, Wiley CA, Achim CL, McCutchan JA (1997) Dendritic injury is a pathological substrate for human immunodeficiency virus—related cognitive disorders. Ann Neurol 42:963–972.

Massud I, Martin A, Dinh C, Mitchell J, Jenkins L, Heneine W, Pau CP, García-Lerma JG (2015) Pharmacokinetic profile of raltegravir, elvitegravir and dolutegravir in plasma and mucosal secretions in rhesus macaques. J Antimicrob Chemother 70:1473–1481.

May MT, Gompels M, Delpech V, Porter K, Orkin C, Kegg S, Hay P, Johnson M, Palfreeman A, Gilson R, Chadwick D, Martin F, Hill T, Walsh J, Post F, Fisher M, Ainsworth J, Jose S, Leen C, Nelson M, et al (2014) Impact on life expectancy of HIV-1 positive individuals of CD4+ cell count and viral load response to antiretroviral therapy. AIDS 28:1193–1202.

McClean J, Nuñez JL (2008) 17α-Estradiol is neuroprotective in male and female rats in a model of early brain injury. Exp Neurol 210:41–50.

McLaurin KA, Li H, Booze RM, Fairchild AJ, Mactutus CF (2018) Unraveling individual differences in the HIV-1 transgenic rat: therapeutic efficacy of methylphenidate. Sci Rep 8:136.

Mendez P, Garcia-Segura LM, Muller D (2011) Estradiol promotes spine growth and synapse formation without affecting pre-established networks. Hippocampus 21:1263–1267.

Michaluk P, Wawrzyniak M, Alot P, Szczot M, Wyrembek P, Mercik K, Medvedev N, Wilczek E, De Roo M, Zuschratter W, Muller D, Wilczynski GM, Mozrzymas JW, Stewart MG, Kaczmarek L, Wlodarczyk J (2011) Influence of matrix metalloproteinase MMP-9 on dendritic spine morphology. J Cell Sci 124:3369–3380.

Milner TA, McEwen BS, Hayashi S, Li CJ, Reagan LP, Alves SE (2001) Ultrastructural evidence that hippocampal alpha estrogen receptors are located at extranuclear sites. J Comp Neurol 429:355–371.

Milner TA, Ayoola K, Drake CT, Herrick SP, Tabori NE, McEwen BS, Warrier S, Alves SE (2005) Ultrastructural localization of estrogen receptor beta immunoreactivity in the rat hippocampal formation. J Comp Neurol 491:81–95.

Moore JP, McKeating JA, Weiss RA, Sattentau QJ (1990) Dissociation of gp120 from HIV-1 virions induced by soluble CD4. Science 250:1139–1142.

Moorjani H, Craddock BP, Morrison SA, Steigbigel RT (1996) Impairment of phagosome-lysosome fusion in HIV-1-infected macrophages. J Acquir Immune Defic Syndr Hum Retrovirol 13:18–22.

Moos WH, Dykens JA, Nohynek D, Rubinchik E, Howell N (2009) Review of the effects of 17α-estradiol in humans: a less feminizing estrogen with neuroprotective potential. Drug Dev Res 70:1–21.

Mukai H, Tsurugizawa T, Murakami G, Kominami S, Ishii H, Ogiue-Ikeda M, Takata N, Tanabe N, Furukawa A, Hojo Y, Ooishi Y, Morrison JH, Janssen WG, Rose JA, Chambon P, Kato S, Izumi S, Yamazaki T, Kimoto T, Kawato S (2007) Rapid modulation of long-term depression and spinogenesis via synaptic estrogen receptors in hippocampal principal neurons. J Neurochem 100:950–967.

Nash B, Tarn K, Irollo E, Luchetta J, Festa L, Halcrow P, Datta G, Geiger JD, Meucci O (2019) Morphine-induced modulation of endolysosomal iron mediates upregulation of ferritin heavy chain in cortical neurons. eNeuro 6:ENEURO.0237-19.2019.

Nath A, Haughey NJ, Jones M, Anderson C, Bell JE, Geiger JD (2000) Synergistic neurotoxicity by human immunodeficiency virus proteins Tat and gp120: protection by memantine. Ann Neurol 47:186–194.

Nikoletopoulou V, Tavernarakis N (2018) Regulation and roles of autophagy at synapses. Trends Cell Biol 28:646–661.

Nixon RA (2013) The role of autophagy in neurodegenerative disease. Nat Med 19:983–997.

Nixon RA (2020) The aging lysosome: an essential catalyst for late-onset neurodegenerative diseases. Biochim Biophys Acta Proteins Proteom 1868:140443.

Norfleet AM, Thomas ML, Gametchu B, Watson CS (1999) Estrogen receptor-α detected on the plasma membrane of aldehyde-fixed GH3/B6/F10 rat pituitary tumor cells by enzyme-linked immunocytochemistry. Endocrinology 140:3805–3814.

Oh SK, Cruikshank WW, Raina J, Blanchard GC, Adler WH, Walker J, Kornfeld H (1992) Identification of HIV-1 envelope glycoprotein in the serum of AIDS and ARC patients. J Acquir Immune Defic Syndr (1988) 5:251–256.

Olivetta E, Arenaccio C, Manfredi F, Anticoli S, Federico M (2016) The contribution of extracellular Nef to HIV-induced pathogenesis. Curr Drug Targets 17:46–53.

Padamsey Z, McGuinness L, Bardo SJ, Reinhart M, Tong R, Hedegaard A, Hart ML, Emptage NJ (2017) Activity-dependent exocytosis of lysosomes regulates the structural plasticity of dendritic spines. Neuron 93:132–146.

Pancera M, Majeed S, Ban YE, Chen L, Huang CC, Kong L, Kwon YD, Stuckey J, Zhou T, Robinson JE, Schief WR, Sodroski J, Wyatt R, Kwong PD (2010) Structure of HIV-1 gp120 with gp41-interactive region reveals layered envelope architecture and basis of conformational mobility. Proc Natl Acad Sci U S A 107:1166–1171.

Pedram A, Razandi M, Lewis M, Hammes S, Levin ER (2014) Membrane-localized estrogen receptor α is required for normal organ development and function. Dev Cell 29:482–490.

Peng J, Vigorito M, Liu X, Zhou D, Wu X, Chang SL (2010) The HIV-1 transgenic rat as a model for HIV-1 infected individuals on HAART. J Neuroimmunol 218:94–101.

Prokai-Tatrai K, Prokai L (2019) A novel prodrug approach for central nervous system-selective estrogen therapy. Molecules 24:4197.

Raybuck JD, Hargus NJ, Thayer SA (2017) A GluN2B-selective NMDAR antagonist reverses synapse loss and cognitive impairment produced by the HIV-1 protein Tat. J Neurosci 37:7837–7847.

Reagan-Shaw S, Nihal M, Ahmad N (2008) Dose translation from animal to human studies revisited. FASEB J 22:659–661.

Reid W, Sadowska M, Denaro F, Rao S, Foulke J, Hayes N, Jones O, Doodnauth D, Davis H, Sill A, O'Driscoll P, Huso D, Fouts T, Lewis G, Hill M, Kamin-Lewis R, Wei C, Ray P, Gallo RC, Reitz M, Bryant J (2001) An HIV-1 transgenic rat that develops HIV-related pathology and immunologic dysfunction. Proc Natl Acad Sci U S A 98:9271–9276.

Reid WC, Ibrahim WG, Denaro F, Casas R, Lee DE, Maric D, Hammoud DA (2016) Characterization of neuropathology in the HIV-1 transgenic rat at different ages. J Neuroimmunol 292:116–125.

Revankar CM, Cimino DF, Sklar LA, Arterburn JB, Prossnitz ER (2005) A transmembrane intracellular estrogen receptor mediates rapid cell signaling. Science 307:1625–1630.

Risher WC, Ustunkaya T, Singh Alvarado J, Eroglu C (2014) Rapid Golgi analysis method for efficient and unbiased classification of dendritic spines. PLoS One 9:e107591.

Royal W, III, Zhang L, Guo M, Jones O, Davis H, Bryant JL (2012) Immune activation, viral gene product expression and neurotoxicity in the HIV-1 transgenic rat. J Neuroimmunol 247:16–24.

Rubin LH, Neigh GN, Sundermann EE, Xu Y, Scully EP, Maki PM (2019) Sex differences in neurocognitive function in adults with HIV: patterns, predictors, and mechanisms. Curr Psychiatry Rep 21:94.

Russell JK, Jones CK, Newhouse PA (2019) The role of estrogen in brain and cognitive aging. Neurotherapeutics 16:649–665.

Ruszczycki B, Szepesi Z, Wilczynski GM, Bijata M, Kalita K, Kaczmarek L, Wlodarczyk J (2012) Sampling issues in quantitative analysis of dendritic spines morphology. BMC Bioinformatics 13:213.

Sá MJ, Madeira MD, Ruela C, Volk B, Mota-Miranda A, Paula-Barbosa MM (2004) Dendritic changes in the hippocampal formation of AIDS patients: a quantitative Golgi study. Acta Neuropathol 107:97–110.

Sacktor N, Skolasky RL, Seaberg E, Munro C, Becker JT, Martin E, Ragin A, Levine A, Miller E (2016) Prevalence of HIV-associated neurocognitive disorders in the Multicenter AIDS Cohort Study. Neurology 86:334–340.

Sampayo RG, Toscani AM, Rubashkin MG, Thi K, Masullo LA, Violi IL, Lakins JN, Cáceres A, Hines WC, Coluccio Leskow F, Stefani FD, Chialvo DR, Bissell MJ, Weaver VM, Simian M (2018) Fibronectin rescues estrogen receptor α from lysosomal degradation in breast cancer cells. J Cell Biol 217:2777–2798.

Santerre M, Arjona SP, Allen CN, Callen S, Buch S, Sawaya BE (2021) HIV-1 Vpr protein impairs lysosome clearance causing SNCA/alpha-synuclein accumulation in neurons. Autophagy 17:1768–1782.

Santosuosso M, Righi E, Lindstrom V, Leblanc PR, Poznansky MC (2009) HIV-1 envelope protein gp120 is present at high concentrations in secondary lymphoid organs of individuals with chronic HIV-1 infection. J Infect Dis 200:1050–1053.

Saxena S, Bucci C, Weis J, Kruttgen A (2005) The small GTPase Rab7 controls the endosomal trafficking and neuritogenic signaling of the nerve growth factor receptor TrkA. J Neurosci 25:10930–10940.

Saylor D, Dickens AM, Sacktor N, Haughey N, Slusher B, Pletnikov M, Mankowski JL, Brown A, Volsky DJ, McArthur JC (2016) HIV-associated neurocognitive disorder–pathogenesis and prospects for treatment. Nat Rev Neurol 12:234–248.

Schlegel A, Wang C, Katzenellenbogen BS, Pestell RG, Lisanti MP (1999) Caveolin-1 potentiates estrogen receptor alpha (ERalpha) signaling. caveolin-1 drives ligand-independent nuclear translocation and activation of ERalpha. J Biol Chem 274:33551–33556.

Schneider J, Kaaden O, Copeland TD, Oroszlan S, Hunsmann G (1986) Shedding and interspecies type sero-reactivity of the envelope glycopolypeptide gp120 of the human immunodeficiency virus. J Gen Virol 67:2533–2538.

Sengupta DC, Lantz CL, Rumi MAK, Quinlan EM (2019) 17α Estradiol promotes plasticity of spared inputs in the adult amblyopic visual cortex. Sci Rep 9:19040.

Sheppard PAS, Choleris E, Galea LAM (2019) Structural plasticity of the hippocampus in response to estrogens in female rodents. Mol Brain 12:22.

Spector SA, Zhou D (2008) Autophagy: an overlooked mechanism of HIV-1 pathogenesis and neuroAIDS? Autophagy 4:704–706.

Speidell A, Asuni GP, Avdoshina V, Scognamiglio S, Forcelli P, Mocchetti I (2019) Reversal of cognitive impairment in gp120 transgenic mice by the removal of the p75 neurotrophin receptor. Front Cell Neurosci 13:398.

Srivastava DP, Waters EM, Mermelstein PG, Kramár EA, Shors TJ, Liu F (2011) Rapid estrogen signaling in the brain: implications for the fine-tuning of neuronal circuitry. J Neurosci 31:16056–16063.

Stout MB, Steyn FJ, Jurczak MJ, Camporez J-PG, Zhu Y, Hawse JR, Jurk D, Palmer AK, Xu M, Pirtskhalava T, Evans GL, de Souza Santos R, Frank AP, White TA, Monroe DG, Singh RJ, Casaclang-Verzosa G, Miller JD, Clegg DJ, LeBrasseur NK, et al (2017) 17α-Estradiol alleviates age-related metabolic and inflammatory dysfunction in male mice without inducing feminization. J Gerontol A Biol Sci Med Sci 72:3–15.

Strong R, Miller RA, Antebi A, Astle CM, Bogue M, Denzel MS, Fernandez E, Flurkey K, Hamilton KL, Lamming DW, Javors MA, de Magalhães JP, Martinez PA, McCord JM, Miller BF, Müller M, Nelson JF, Ndukum J, Rainger GE, Richardson A, et al (2016) Longer lifespan in male mice treated with a weakly estrogenic agonist, an antioxidant, an α-glucosidase inhibitor or a Nrf2-inducer. Aging Cell 15:872–884.

Sundermann EE, Heaton RK, Pasipanodya E, Moore RC, Paolillo EW, Rubin LH, Ellis R, Moore DJ (2018) Sex differences in HIV-associated cognitive impairment. AIDS 32:2719–2726.

Szotek EL, Narasipura SD, Al-Harthi L (2013) 17β-Estradiol inhibits HIV-1 by inducing a complex formation between β-catenin and estrogen receptor α on the HIV promoter to suppress HIV transcription. Virology 443:375–383.

Toran-Allerand CD, Tinnikov AA, Singh RJ, Nethrapalli IS (2005) 17α-Estradiol: a brain-active estrogen? Endocrinology 146:3843–3850.

Totta P, Pesiri V, Marino M, Acconcia F (2014) Lysosomal function is involved in 17β-estradiol-induced estrogen receptor α degradation and cell proliferation. PLoS One 9:e94880.

Trujillo JR, Navia BA, Worth J, Lucey DR, McLane MF, Lee TH, Essex M (1996) High levels of anti-HIV-1 envelope antibodies in cerebrospinal fluid as compared to serum from patients with AIDS dementia complex. J Acquir Immune Defic Syndr Hum Retrovirol 12:19–25.

Tsuruta F, Dolmetsch RE (2015) PIKfyve mediates the motility of late endosomes and lysosomes in neuronal dendrites. Neurosci Lett 605:18–23.

Wang AC, Hara Y, Janssen WG, Rapp PR, Morrison JH (2010) Synaptic estrogen receptor-alpha levels in prefrontal cortex in female rhesus monkeys and their correlation with cognitive performance. J Neurosci 30:12770–12776.

Wenzel ED, Bachis A, Avdoshina V, Taraballi F, Tasciotti E, Mocchetti I (2017) Endocytic trafficking of HIV gp120 is mediated by dynamin and plays a role in gp120 neurotoxicity. J Neuroimmune Pharmacol 12:492–503.

Wilson ME, Allred KF, Bisotti AJ, Bruce-Keller A, Chuahan A, Nath A (2006) Estradiol negatively regulates HIV-LTR promoter activity in glial cells. AIDS Res Hum Retroviruses 22:350–356.

Yang SH, Liu R, Perez EJ, Wen Y, Stevens SM Jr, Valencia T, Brun-Zinkernagel AM, Prokai L, Will Y, Dykens J, Koulen P, Simpkins JW (2004) Mitochondrial localization of estrogen receptor beta. Proc Natl Acad Sci U S A 101:4130–4135.

Yap CC, Digilio L, McMahon LP, Garcia ADR, Winckler B (2018) Degradation of dendritic cargos requires Rab7-dependent transport to somatic lysosomes. J Cell Biol 217:3141–3159.

Yoo KS, Lee K, Oh JY, Lee H, Park H, Park YS, Kim HK (2019) Postsynaptic density protein 95 (PSD-95) is transported by KIF5 to dendritic regions. Mol Brain 12:97.

Zemlyak I, Brooke S, Sapolsky R (2005) Estrogenic protection against gp120 neurotoxicity: role of microglia. Brain Res 1046:130–136.

Zhong F, Liu L, Wei J-L, Dai R-P (2019) Step by step Golgi-Cox staining for cryosection. Front Neuroanat 13:62.

Zhou D, Spector SA (2008) Human immunodeficiency virus type-1 infection inhibits autophagy. AIDS 22:695–699.